Lawrence Berkeley Laboratory
UNIVERSITY OF CALIFORNIA

ENERGY & ENVIRONMENT DIVISION

ATMOSPHERIC AEROSOL RESEARCH FY-1979

Chapter in the Energy and Environment Annual Report, 1979

Atmospheric Aerosol Research Group

July 1980

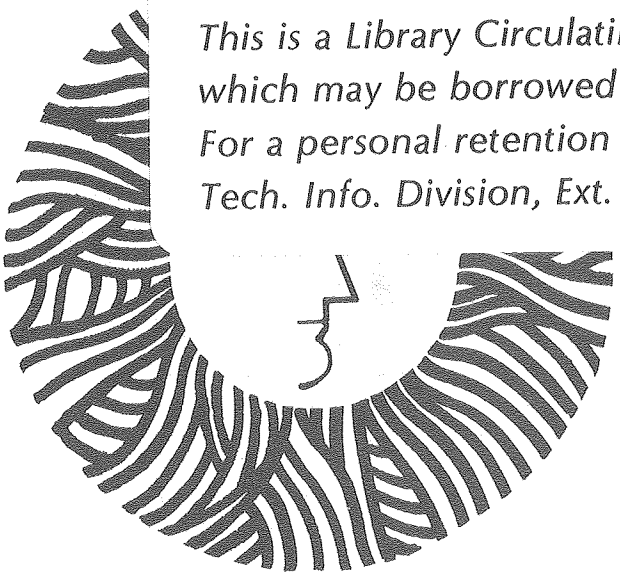

Prepared for the U.S. Department of Energy under Contract W-7405-ENG-48

DISCLAIMER

CONTENTS

ATMOSPHERIC AEROSOL RESEARCH

INTRODUCTION

T. Novakov

The complex set of questions concerning the origin and the chemical and physical characterization of carbonaceous particulates and their role in atmospheric chemistry has been central to the program of the Atmospheric Aerosol Research group since the group's beginning in 1972. As a result of this research, our group advanced the hypothesis that much of the carbonaceous material in urban environments is soot, i.e., primary particulate material. These preliminary results on the origin and nature of carbonaceous particles were first reported at the First Annual NSF Trace Contaminants Conference at Oak Ridge National Laboratory in August 1973, just one year after the start of our research, which was at that time entirely sponsored by the National Science Foundation.

Carbonaceous particles, together with sulfur and nitrogen compounds, account for most of the submicron particulate mass. Of the above species, particulate carbon is often the most abundant material found in urban environments (e.g., Los Angeles, Denver, New York). According to the view prevailing at the time our research was initiated, it was postulated that most of the particulate material was produced by certain atmospheric photochemical reactions from gaseous hydrocarbons. The products of these reactions were believed to be certain highly oxygenated high molecular weight hydrocarbons which condense into carbonaceous particles. More specifically, reactions of ozone with olefinic hydrocarbon vapors were assumed to be the principal mechanism for such gas-to-particle conversion processes. The principal ingredient necessary for these reactions is ozone, which--according to some investigations--has to exist in concentrations exceeding about 0.2 ppm.

In contrast, the view emerging from our work has suggested that most of the particulate carbon is either directly of primary origin or contains, in addition, secondary carbonaceous material produced in nonphotochemical reactions--for example, surface reactions that involve primary particles. It is clear that the control technology and strategy for the abatement of carbonaceous particulates will depend on the relative importance of these two alternative pathways for the formation of carbonaceous species.

Primary soot particles are not only a major constituent of ambient particles but also are a catalytically and surface chemically active material that could be responsible for the formation of sulfates resulting from fossil fuel combustion. Following is a review of recent work performed by the Atmospheric Aerosol Research group, which further stresses the importance of primary particles in the atmosphere.

Funding for this work is from the Department of Energy--Division of Biomedical and Environmental Research, the National Science Foundation, and the Environmental Protection Agency.

CARBON-CATALYZED REACTIONS IN AQUEOUS SUSPENSIONS: OXIDATION OF SO_2 AT LOW CONCENTRATIONS*

R. Brodzinsky, et al.

INTRODUCTION

Activated carbon, because of its adsorptive properties, has long been used as a scrubber for gases and organic molecules. It is also used as a catalyst in industry for the control of gaseous emissions from smoke stacks. The catalytic oxidation of SO_2 on activated carbons has been shown to occur[1] and has been used in certain industrial scrubber processes.[2] Novakov et al.[3,4] have shown by photoelectron spectroscopy that SO_2 oxidation can be catalyzed by combustion-generated soot particles. These studies indicated that the soot-catalyzed reaction is more efficient in prehumidified air than in dry air, but the specific role of water was not clear from their experiments.

Environmentally, this soot-catalyzed reaction may be extremely important as soot particles are a major constituent of the ambient particulate burden.[3] The effects of liquid water on the reaction are important because the water may condense on soot particles in plumes as the particles pass through clouds and fog.

We have extended the research on the role of soot particles as catalysts for SO_2 oxidation by studying the effect of liquid water on the carbon-catalyzed reaction.[5] In that paper we studied the roles of the activated carbon surface, oxygen, temperature, and pH. The results of that study are summarized as follows:

1. The reaction rate is first order and 0.69^{th} order with respect to the concentration of carbon and dissolved oxygen respectively.

2. The reaction rate is effectively pH independent (pH < 7.6).

3. The activation energy of the reaction is 11.7 kcal/mole.

4. There is a mass balance between the consumption of sulfurous acid and the production of sulfuric acid.

The dependence of the reaction rate on the concentration of sulfurous acid was not seen since only a narrow concentration range (10^{-4} - 10^{-3} M) was used. In this range, the reaction rate is independent of sulfurous acid concentration.

In this paper we present the results of the effects that the concentration of S(IV) species have on the reaction rate, a reaction rate law, and a proposed reaction mechanism for the catalytic oxidation of SO_2 on carbon particles in an aqueous suspension. (Note: Because, in solution, SO_2 can form the three species $SO_2 \cdot H_2O$, HSO_3^- (bisulfite), and $SO_3^=$ (sulfite), the terms "sulfurous acid" and "H_2SO_3" have been used to signify all of the S(IV) species in solution.)

EXPERIMENTAL METHODS AND RESULTS

As in the previous studies, an activated carbon (Nuchar C-190, a trademark of West Virginia Pulp and Paper Co.) was used as a model system since it is difficult to prepare soot suspensions reproducibly. A Dionex Model 14 anion chromatography system was used for sulfurous acid and sulfate concentrations of less than 10^{-4} M. An eluent of 0.002 M NaOH/ 0.0035 M Na_2CO_3 at a flow rate of 138 ml/hr and pressure of 600 psi, through a system consisting of a 3 x 50 mm concentrator, 3 x 150 mm precolumn, 3 x 500 mm separator, and 6 x 250 mm suppressor columns was used. The sulfite peak eluted at 10 minutes with sulfate following at 15. Iodometric titrations were used to determine sulfurous acid concentrations above 10^{-4} M, as in the previous experiments. The pH of the solution was varied in the range of 4.0 to 7.5 for the experiments done on the ion chromatograph.

Figure 1 shows the effective rate of reaction (normalized carbon concentration, room temperature (20°C), and air) versus the sulfurous acid concentration. The data points are the instantaneous rates based on three-point averages from the various experiments. The rate of reaction is second order with respect to H_2SO_3 below 10^{-7} M, moves through a first order reaction around 5 x 10^{-6} M, and becomes independent of H_2SO_3 concentrations above 10^{-4} M.

This behavior may be summarized and added to our previous four results as:

5. The reaction rate has a complex dependence on the concentration of H_2SO_3, ranging between a second and zeroth order reaction.

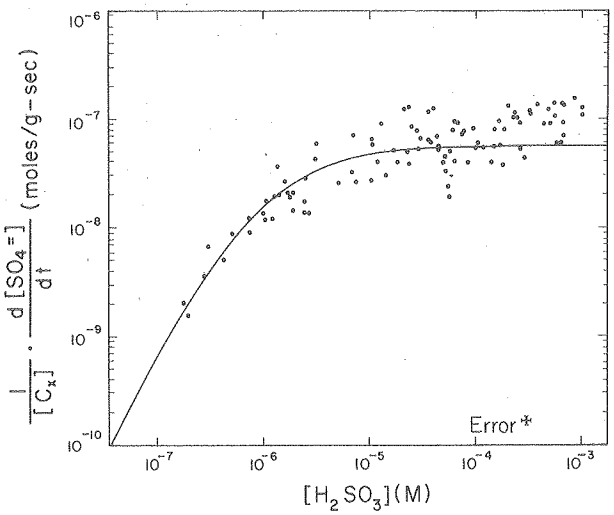

Fig. 1. Effective rate of reaction vs $[H_2SO_3]$. Curve is least squares fit to proposed rate expression. (XBL 7911-13280)

DISCUSSION

The oxidation of S(IV) to S(VI) can be expressed simply by the symbolic net reaction,

$$2S(IV) + O_2 \rightarrow 2S(VI) \quad .$$

(For this and following reactions, let C_x = carbon surface; S(IV) = $H_2O \cdot SO_2$, HSO_3^-, and $SO_3^=$; S(VI) = HSO_4^-, and $SO_4^=$.)

The experimental results yield the following empirical rate law for this reaction:

$$\frac{d[S(VI)]}{dt} = k[C_x][O_2]^{0.69} \frac{\alpha[S(IV)]^2}{1 + \beta[S(IV)] + \alpha[S(IV)]^2} \qquad (I)$$

where $k = 1.69 \times 10^{-5}$ moles$^{.31} \cdot \ell^{.69}/g \cdot sec$

$\alpha = 1.50 \times 10^{12} \ell^2/mole^2$

$\beta = 3.06 \times 10^6$ ℓ/mole

$[C_x]$ = grams of Nuchar C-190/ℓ,

$[O_2]$ = moles of dissolved oxygen/ℓ, and

[S(IV)] = total moles of S(IV)/ℓ.

Using the Arrhenius equation, the rate constant may be expressed as

$$k = Ae^{-E_a/RT}$$

where $E_a = 11.7$ kcal/mole

and $A = 9.04 \times 10^3$ moles$^{.31} \cdot \ell^{.69}/g \cdot sec$

The reaction rate being first order with respect to the activated carbon catalyst is representative of a surface catalysis. The reaction will then proceed via the adsorption of the reaction species onto a catalytically active site. A series of adsorption steps can explain the fractional and varying order of reaction with respect to O_2 and S(IV) and are proposed here in the following four-step reaction:

$$C_x + O_2 \underset{k_{-1}}{\overset{k_1}{\rightleftarrows}} C_x \cdot O_2 \qquad (1)$$

$$C_x \cdot O_2 + S(IV) \underset{k_{-2}}{\overset{k_2}{\rightleftarrows}} C_x \cdot O_2 \cdot S(IV) \qquad (2)$$

$$C_x \cdot O_2 \cdot S(IV) + S(IV) \underset{k_{-3}}{\overset{k_3}{\rightleftarrows}} C_x \cdot O_2 \cdot S^2(IV) \qquad (3)$$

$$C_x \cdot O_2 \cdot S^2(IV) \xrightarrow{k_4} C_x + 2\ S(VI) \qquad (4)$$

With the Langmuir adsorption equation, the following is arrived at for the rate expression:

$$\frac{d[S(VI)]}{dt} = 2k_4[C_x] \left[\frac{K_1[O_2]}{1+K_1 O_2}\right] \left[\frac{K_2\ S(IV)}{1+K_2\ S(IV)}\right] \left[\frac{K_3\ S(IV)}{1+K_3\ S(IV)}\right]$$

where $K_1 = k_1/k_{-1}$, $K_2 = k_2/k_{-2}$, $K_3 = k_3/k_{-3}$.

Equation II can be changed simply to Equation I. A fractional order adsorption reaction is achieved by substituting the Freundlich isotherm

$$\theta = k[X]^n \quad ,$$

where θ is the fraction of the surface covered by adsorbed species X, for the Langmuir isotherm[6]

$$\theta = \frac{K[X]}{1 + K[X]} \quad .$$

Multiplication of the S(IV) terms yields the experimentally seen expression, where $K_2K_3 = \alpha$ and $K_2 + K_3 = \beta$.

Preliminary experiments with other activated carbons, as well as laboratory-generated combustion soots, have shown the same rate law behavior, while the actual numerical constants are different. This behavior has also been reproduced using coal fly ash samples, which have a low percentage of carbon. An activated surface-catalyzed reaction can be very important in the plumes of coal-fired plants, even in the absence of carbonaceous soot.

We have done comparisons of this reaction with the rates of the other atmospherically important SO_2 oxidation reactions.[7] It is clear that the carbon-catalyzed reaction can be a major contributor to the formation of aerosol sulfates.

FOOTNOTE AND REFERENCES

*Condensed from Lawrence Berkeley Laboratory Report, LBL-10488 (1980) (Submitted to Journal of Physical Chemistry.)

1. J. Siedlewski, "The mechanism of catalytic oxidation on activated carbon: The influence of free carbon radicals on the adsorption of SO_2," Int. Chem. Eng. 5, 297 (1965).

2. M. Hartman and R. W. Coughlin, "Oxidation of SO_2 in a trickle-bed reactor packed with carbon," Chem. Eng. Sci. 27, 867 (1972).

3. T. Novakov, S. G. Chang, and A. B. Harker, "Sulfates as pollution particulates: Catalytic formation on carbon (soot) particles," Science 186, 259 (1974).

4. T. Novakov, S. G. Chang, R. L. Dod, "Application of ESCA to the analysis of atmospheric particulates," in Contemporary Topics in Analytical and Clinical Chemistry - Vol. I, D. M. Hercules, G. M. Hieftje, L. R. Snyder, and M. A. Evenson, eds. (New York, Plenum, 1977), p. 249.

5. R. Brodzinsky, S. G. Chang, S. S. Markowitz, and T. Novakov, "Kinetics and mechanism for the catalytic oxidation of SO_2 on carbon in aqueous suspensions," in Atmospheric Aerosol Research Annual Report, 1977-78, Lawrence Berkeley Laboratory Report LBL-8696 (1978).

6. S. W. Benson, The Foundations of Chemical Kinetics (New York, McGraw-Hill, 1960), p. 624.

7. S. G. Chang, R. Brodzinsky, R. Toossi, S. S. Markowitz, and T. Novakov, "Catalytic oxidation of SO_2 on carbon in aqueous suspensions," in Proceedings of the Conference on Carbonaceous Particles in the Atmosphere, Lawrence Berkeley Laboratory Report LBL-9037, p. 122 (1979).

REDUCTION OF NO_x BY SO_2 IN AQUEOUS SOLUTION*

S. Oblath, et al.

INTRODUCTION

The oxides of both sulfur and nitrogen are abundant and well-studied atmospheric pollutants. The interaction of the two has been previously studied only in the gas phase.[1-3] Although liquid water is present in clouds, fogs, plumes, and the human respiratory system, atmospheric chemists have not yet investigated reactions of SO_2 and NO_x after dissolution into water. In addition, these aqueous reactions need investigation because deliquescent salts such as NH_4HSO_4 can pick up liquid water at a low relative humidity.[4]

Previous investigations of the reactions of NO_x with SO_2 in aqueous solutions revealed many competing reactions.[5,6] Nitric, nitrous and sulfurous acids are the immediate products upon dissolution of the gases. Nitric acid reacts with sulfurous acid to form nitrosylsulfuric acid.[6] Nitrous acid can be reduced by sulfurous acid to produce nitrogen species such as N_2O, N_2, NH_3, hydroxylamine sulfonates and amine sulfonates while sulfurous acid is oxidized to sulfuric acid. A summary of the reactions and products formed is shown in Fig. 1. The kinetics and mechanisms of these reactions have not been well characterized. Nevertheless, it has been demonstrated that the products of the reaction depend on the concentrations of reactants, temperature, and acidity of the solution.

Because the formation of hydroxylamine disulfonate (HADS) is the first step to any of the products when nitrous acid reacts with sulfurous acid under most atmospheric conditions, investigating the kinetics of HADS is essential to any attempt at assessing the importance of this system as a sink of NO_x and as a source of sulfate and reduced nitrogen species.

Previous work determined the order of reaction with respect to nitrite, bisulfite, and hydrogen ion. The results showed reactions first order in nitrite at all pH's, first order in bisulfite at pH of 4.5 and 5.5, and second order in bisulfite at pH of 7.[7] Experiments have been carried out this year to determine the pH, temperature, and ionic strength dependencies of the reaction and a mass balance for nitrogen species. A reaction rate law has been obtained and a mechanism is proposed.

EXPERIMENTAL METHODS AND RESULTS

The study has been carried out by reacting NO_2^- and HSO_3^- in various buffers to have a well-characterized system. The reaction is monitored by spectrophotometric determination of NO_2^-. Sulfur (IV) species were monitored by standard iodometric techniques. Concentrations were varied between 5-30 millimolar in NO_2^-, 20-200 millimolar in HSO_3^-, and 10^{-7} to 10^{-4} molar in H^+.

Experiments have been made to determine pH dependence on the reaction. The process first order in bisulfite shows a first order H^+ ion dependence.[7] The second order portion, which is predominant at pH of 7, is independent of hydrogen ion and sulfite concentrations. The results are shown in Table 1.

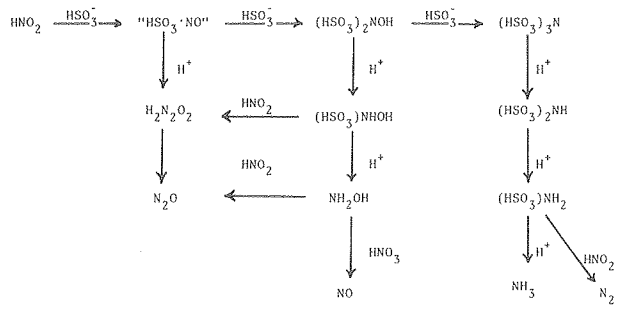

Fig. 1. Reaction scheme for the reduction of nitrite with bisulfite. Species in quotes has been postulated but not yet observed.

Table 1. Typical runs to determine pH dependence at $\mu = 1.2$ for second order process.

Run #	$[NO_2^-]^a$	$[HSO_3^-]^a$	$[SO_3^=]^a$	pH	$\frac{d \ln[NO_2^-]^b}{dt}$ Total	1st order	2nd order
1	0.010	0.10	0.10	6.53	0.0136	0.0074	0.0062
2	0.010	0.10	0.20	6.85	0.0102	0.0035	0.0067
3	0.015	0.10	0.15	6.73	0.0114	0.0047	0.0067
4	0.015	0.10	0.15	6.71	0.0112	0.0049	0.0063
5	0.015	0.20	0.10	6.30	0.0492	0.0251	0.0241
6	0.015	0.20	0.20	6.58	0.0364	0.0132	0.0232
7	0.015	0.20	0.15	6.46	0.0395	0.0173	0.0222
8	0.015	0.25	0.10	6.25	0.0680	0.0351	0.0329
9	0.015	0.25	0.20	6.52	0.0569	0.0189	0.0380
10	0.015	0.25	0.15	6.38	0.0601	0.0261	0.0340

[a] concentrations in moles/liter

[b] rates in $min.^{-1}$

The temperature dependence of the reaction was investigated by varying the temperature by means of a water bath. The rest of the experimental conditions were not varied. For the runs at low pH (4.5), the reaction was found to vary with temperature, as can be seen by the results in Fig. 2. The activation energy from this study is 12.1 kcal/mole, in good agreement with the literature.[8] A similar set of runs for the second order process reveals that it is nearly independent of temperature.

Further experiments were done to find the ionic strength (μ) dependence of the reaction. This was accomplished by varying ionic strength upon addition of $NaNO_3$ and Na_2SO_4. The first order process shows no dependence on ionic strength. The second order process shows a marked dependence, which is presented in Fig. 3.

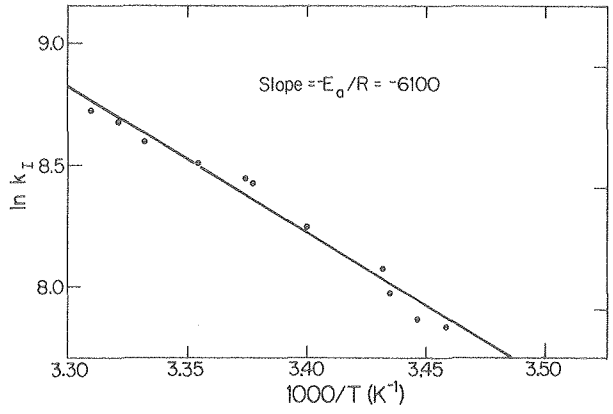

Fig. 2. Arrhenius plot showing temperature dependence of the rate constant for the process first order in bisulfite. (XBL 7911-13319)

Final experiments were carried out to determine a mass balance for nitrogen species. HADS was measured spectrophotometrically after oxidation to nitrosodisulfonate.[9] Results are shown in Fig. 4, indicating that HADS is the major product in the reaction. Hydrolysis and sulfonation reactions caused the apparent loss of nitrogen species.

DISCUSSION

The data indicate that there are two concurrent processes for the formation of HADS. This can be stated in the experimental rate law.

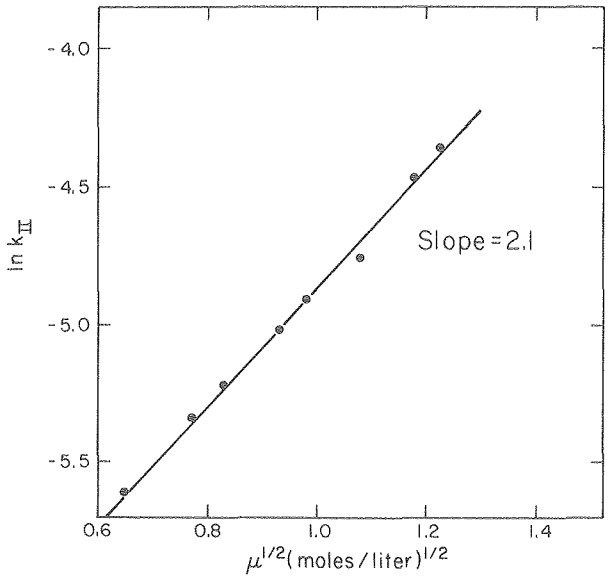

Fig. 3. Dependence of the rate constant for the process second order in bisulfite on the ionic strength. (XBL 7911-13320)

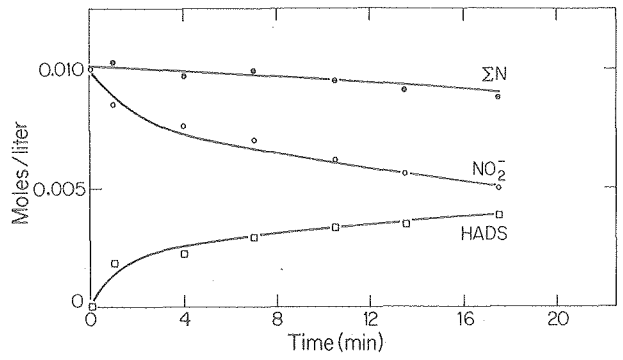

Fig. 4. Mass balance for nitrogen species. Σ N represents the sum of nitrite and HADS. (XBL 7911-13321)

$$\text{Rate} = k_1(H^+)(NO_2^-)(HSO_3^-) + k_2(HSO_3^-)^2(NO_2^-) \quad ,$$

$$\text{where } k_1 = (2.2\times10^{14})e^{-6100/T}\ \frac{\text{liter}^2}{\text{mole}^2\text{min}}$$

$$\text{and} \quad k_2 = (5.4\times10^{-2})e^{2.2\sqrt{\mu}}\ \frac{\text{liter}^2}{\text{mole}^2\text{min}} \quad .$$

Since there are a limited number of sulfur species present and the restriction that the two processes cannot have the same intermediate, we propose the following mechanism:

1) $H^+ + NO_2^- = HNO_2$ fast equilibrium

2) $NO_2^- + S_2O_5^{=} = NO(SO_3)_2^{-3}$

3) $HNO_2 + HSO_3^- = NOSO_3^- + H_2O$

4) $NOSO_3^- + HSO_3^- = NOH(SO_3)_2^{-2}$

Since $NOSO_3^-$ has never been detected, we can assume it is in a small steady state concentration. Using this steady state assumption, and looking only at the rate expression for the initial reaction times, we get the following rate expression,

$$\text{Rate} = k_A(HONO)(HSO_3^-) + k_B(NO_2^-)(HSO_3^-)^2 \quad ,$$

which is identical in form to the observed rate law.

The ionic strength data for this mechanism fit exactly as expected from Debye-Huckel Theory. However, because of the breakdown of the theory at these higher ionic strengths, these are tentative conclusions. The fact that the second order process does not correlate to either H^+ or $SO_3^{=}$ concentration but only to HSO_3^- lends credence to $S_2O_5^{=}$ as the reacting species. The first order process correlates equally well with sulfur (IV) and HSO_3^-, as would be expected since HSO_3^- is the major species.

The significance of this reaction in terms of atmospheric aerosol production is the formation of sulfate and reduced nitrogen-containing sulfonates. The sulfate comes from each of the hydrolysis steps in the scheme in Fig. 1. In addition, gaseous species such as NO, N_2O, N_2, or NH_3 could form as a result of the interaction between nitrous acid and sulfurous acid. The extent to which these gaseous species are produced depends on the condition of the reaction. One of the major obstacles to evaluating this reaction is that there are limited data on the nitrous acid concentration in water under atmospheric or plume conditions. There are indications, however, that under these conditions, a considerable amount of nitrite is found,[10] which clearly indicates a need for an understanding of these reactions.

FOOTNOTE AND REFERENCES

*Condensed from Lawrence Berkeley Laboratory Report, LBL-10504 (1980). (Submitted to Journal of Physical Chemistry.)

1. R. P. Urone, H. Lutsep, C. M. Noyes, and J. F. Parcher, "Static studies of sulfur dioxide reactions in air," Environ. Sci. Technol. 2, 611 (1968).

2. A. P. Altshuller and J. Bufalini, "Photochemical aspects of air pollution: A review," Environ. Sci. Tech. 5. 39 (1971).

3. J. G. Calvert, F. Su, J. W. Bottenheim, and O. P. Strausz, "Mechanism of the homogeneous oxidation of sulfur dioxide in the troposphere," Atmos. Environ. 12, 197 (1978).

4. R. J. Charlson, D. S. Covert, T. V. Larson, and A. P. Waggoner, "Chemical properties of tropospheric sulfur aerosols," Atmos. Environ. 12, 39 (1978).

5. F. Rashcig, Schwefel und Stickstoffstudien (Verlag Chemie, Berlin, 1924).

6. W. Latimer and J. Hildebrand, Reference Book of Inorganic Chemistry (New York, MacMillan, 1951), p. 208.

7. S. B. Oblath, S. S. Markowitz, T. Novakov, and S. G. Chang, "Kinetics and mechanism of the reactions of NO_x with SO_2 in aqueous solutions," in Atmospheric Aerosol Research Annual Report, 1977-78, Lawrence Berkeley Laboratory Report LBL-8696 (1978).

8. S. Yamamoto and T. Kaneda, "Kinetics of formation of hydroxylaminedisulfonate and nitrilosulfonate by Raschig's hydroxylamine process," Nippon Kagaku Zasshi 80, 1098 (1959).

9. V. F. Seel and E. Degener, "Kinetik und Chemismus der Raschigschen Hydroxylamin-Synthese," Z. Anorg. Allg. Chem. 284, 100 (1956).

10. H. J. Crecelius and W. Forwerg, "Untersuchungen zum 'Saltzman-Faktor'," Staub-Reinhalt Luft 30, 294 (1970).

SULFATE FORMATION BY COMBUSTION PARTICLES IN A LABORATORY FOG CHAMBER

W. Benner, et al.

INTRODUCTION

Particulate sulfate can compose a significant fraction of the total suspended particulate material in urban air and has been implicated in visibility reduction and as the cause of the characteristic low pH observed in acid rain.[1] Inhaled sulfate can also pose a health hazard, but the severity of the health threat is not clear. The description of the chemical and physical processes which introduce sulfate into the atmosphere is being revised constantly. Recent attention has been directed towards sulfate formation pathways which involve liquid water. The work reported here focuses on a pathway in which SO_2 is oxidized by dispersed water droplets such as those found in plumes, clouds, and fogs.

Work in our laboratory plus recent literature suggests that liquid water is an important component in the mechanism by which SO_2 is oxidized in the ambient air. Penkett et al.[2] calculated that the oxidation of SO_2 by O_3 and/or H_2O_2 in cloud droplets can lead to sulfate formation. Wolff et al.[3] present ambient sampling data suggesting that particulate sulfate is formed by two mechanisms: one involving photochemical oxidation, the other proceeded by an O_3-fog droplet route. Enger and Hogstrom[4] found that the rate of SO_2 oxidation in a power plant plume increases when the plume relative humidity (RH) is high. Johnstone and Mall[5] studied SO_2 oxidation in a laboratory fog chamber and found that SO_2 is oxidized rapidly when the droplets contain Mn^{+2}. Dittenhoefer and de Pena[6] report that after a relatively dry power plant plume merged with a nearly saturated cooling tower plume, sulfate formed on the power plant plume particles. Work in our laboratory has shown that aqueous suspensions of soot particles can oxidize SO_2 rapidly.[7] Earlier fog chamber studies in our laboratory indicated that dispersed water droplets which contain soot nuclei can also oxidize SO_2.[8]

It is hypothesized that under certain meteorological conditions, soot particles in the ambient air can become sites for SO_2 oxidation; this reaction pathway needs additional investigation. The work reported here is a continuation of our laboratory investigation concerning oxidation of SO_2 by water encapsulated soot particles. This year's work was conducted in an improved experimental system in which a new fog chamber and a new gas burner and associated sampling devices could be operated under conditions more properly controlled than previously possible in earlier fog chamber studies.[8]

EXPERIMENTAL

Figure 1 shows a diagram of the experimental system. The fog chamber is 15 cm i.d. x 2.4 m tall and was constructed from stainless steel pipe with plexiglass end-caps. A 1-mW He-Ne laser beam is directed downward through the top plexiglass end-cap and is used to visually judge the fog density.

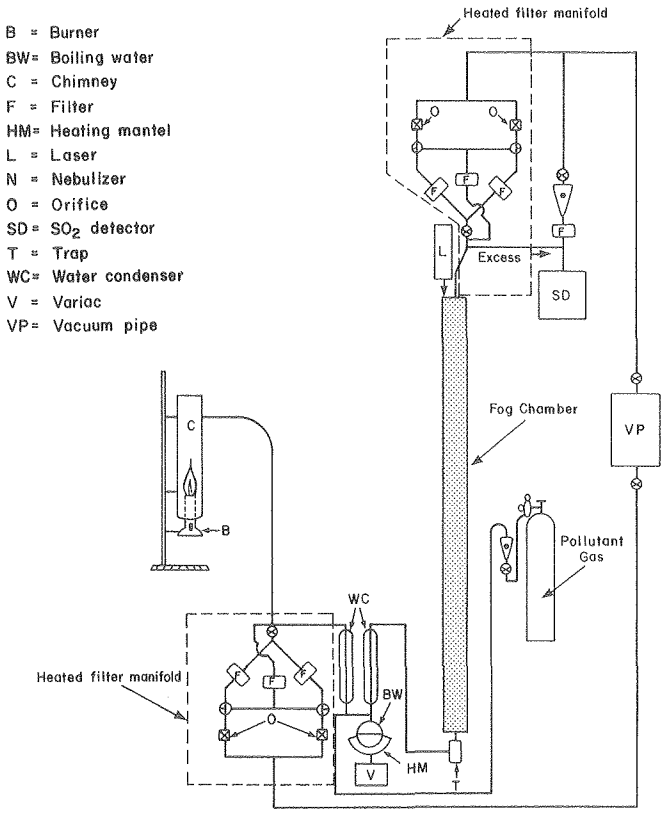

Fig. 1. Fog chambers and associated equipment used to study the oxidation of SO_2 by fog droplets which contain combustion nuclei. The filters were heated to ~45°C. (XBL 804-4123)

Pipeline natural gas is burned (~2 L/min) in a Fisher-type Bunsen burner. A diffusion flame is produced by covering the air holes at the burner base, and a premixed flame results when the air holes are open. The premixed flames produce many combustion particles which nucleate water, but these particles are not sooty and do not produce a gray deposit when collected on filters. The diffusion flames produce many black soot particles which nucleate water. The combustion gases from the burner are directed into an 8 cm i.d. x 40 cm tall stainless steel chimney. A portion of the combustion gases is withdrawn from the chimney and then drawn through the fog generator (humidifier and condensers) and finally through the vertical fog chamber. The flow rate of gases and particles through the chamber was held constant, and thus the time during which the droplets could react with SO_2 was the same for all runs. The reaction time or droplet residence time in the fog chamber was ~15 min. SO_2 (205 ppm SO_2 in N_2) can be introduced into the air stream before water is condensed onto the soot particles.

Filter samples of fresh soot particles, i.e., particles before exposure to fog and SO_2, and fog droplets withdrawn from the top of the chamber can be collected simultaneously. Samples are collected on 0.5-μm pore Fluoropore filters and prefired quartz fiber filters. The filter holders are heated to ~45°C to prevent liquid water from collecting on the filters. This precaution precludes the possibility of chemical reactions involving liquid water occurring on the filter media. An SO_2 specific detector (Thermo Electron Corp.) is used to continuously monitor the SO_2 concentrations in the chamber. A 12-stage impactor can be used in place of the filters to collect samples of either fresh soot particles or fog droplets from the top of the chamber. Prefired quartz filters are used as the impaction surfaces and the after-filter in the impactor.

Pieces of the particle-laden quartz filters were analyzed for total carbon by a combustion technique which converted the carbon on the filter to CO_2, and the resultant CO_2 was quantitated by infrared spectroscopy. Separate pieces of the quartz filters were extracted by sonication in water, and the extract was then filtered through a pre-extracted 0.22-μm pore Millipore filter. The filtered extract was analyzed by ion chromatography. To correct for artifact formation, i.e., the conversion of SO_2 to sulfate by the dry quartz filters, two back-to-back quartz filters were used during sample collection, and thereby the concentrations of anions on the backup filter could be subtracted from those concentrations found on the front (particle-laden) filter. We eventually switched to Fluoropore filters instead of quartz filters because background concentrations and artifact formation were negligible on the Fluoropore filters. Extracts of the Fluoropore filters were obtained by placing pieces of the filter, along with some water, in a capped test tube and vigorously shaking the tube on a motor-driven shaker. This extract was subsequently filtered through a pre-extracted 0.22-μm pore Millipore filter and then analyzed by ion chromatography.

An ion chromatograph (Dionex Corp., Sunnyvale, California) was used to quantitate the concentrations of NO_2^-, NO_3^-, $SO_3^=$, and $SO_4^=$ in the filter extracts. Several mL of filter extract were injected onto an anion concentrator column. A flow of ~140 mL/min (30% flow) of 0.002 M NaOH + 0.0035 M Na_2CO_3 was then directed through the concentrator column, and the displaced anions were separated on a 3 x 500 mm separator column; a 6 x 250 mm suppressor column was used to lower the conductivity of the eluent so that the separated anions could be detected by conductimetry. Various dilutions of a mixed standard solution of NO_2^-, NO_3^-, $SO_3^=$, and $SO_4^=$ were injected separately and a graph of signal (peak height in micromhos) vs. weight was plotted for each anion. The concentration of an anion in a sample was obtained by comparing its peak height to the proper standard curve.

RESULTS AND DISCUSSION

The collection of particles in the cascade impactor revealed that ~20% of the soot particles on a weight basis were covered with water. This finding is shown in Fig. 2. The curve labeled Soot in Fig. 2 is the mass size distribution for fresh soot particles and shows that few particles are larger than ~2 μm diameter. The curve labeled Fog in Fig. 2 shows the mass size distribution of the wet soot particles. The fog caused some of the soot particles to shift to a larger size range. This size shift is due to at least two processes. First, the soot particles served as centers onto which liquid water condenses and second, Brownian diffusion causes some of the soot particles to collide with fog droplets and become incorporated into the droplets. The stages on the impactor which collected fog droplets, i.e., 2- to 10-μm diameter size range, became wet and gray, indicating the concurrence of soot particles and fog droplets. The ratio for the carbon in the 2- to 10-μm diameter range (fog droplets) to the total carbon for curve F is 0.2. This ratio indicates that for conditions used, not enough water was available to cover all the soot particles with an equal amount of liquid water. The Kelvin effect, which states that the vapor pressure above a curved surface increases as the curvature increases, is an influencing factor which determines which particles become condensation nuclei. This effect would cause the larger soot particles to become condensation nuclei preferentially over smaller soot particles because the larger ones have less curvature and can thus condense water at a lower supersaturation ratio than that ratio required by smaller particles. The surface properties of the particles can also influence condensation. We have hypothesized that the wet soot particles are the ones which oxidize SO_2 to sulfate, but definitive experimental data are not available. If only the wet soot particles cause sulfate formation, then the fraction of soot particles which are wet is an important consideration in those experimental runs. On-going experiments are, in part, directed towards answering this question.

Chemical analysis of filter samples collected from the fog chamber showed that SO_2 was easily oxidized by wet soot particles. The results of the filter analysis are presented in Fig. 3. Net sulfate produced equals $[\overline{SO_4^=}]$ fog - $[\overline{SO_4^=}]$ fresh

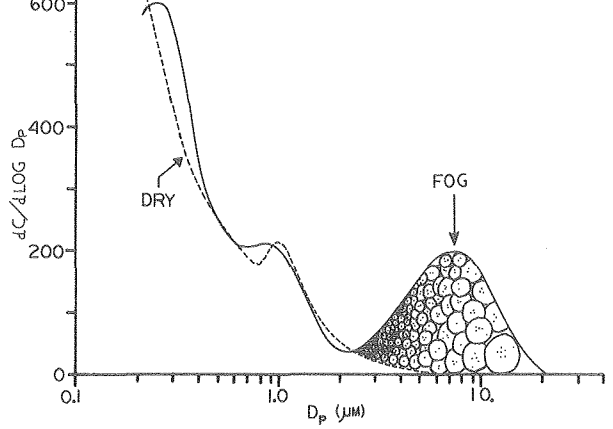

Fig. 2. Particle size distributions of fog chamber particles. (XBL 799-11295)

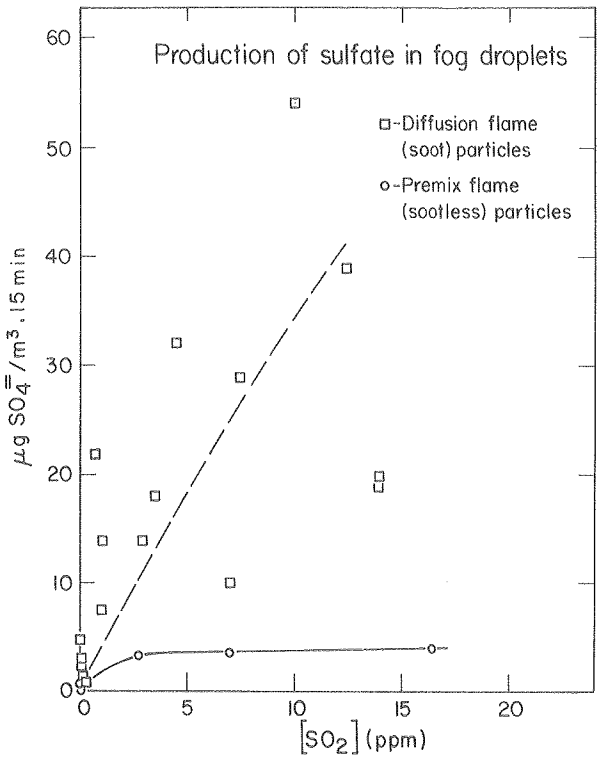

Fig. 3. Net sulfate produced by wet combustion particles exposed to SO_2. The sulfate values correspond to a droplet reaction time of 15 min. (XBL 804-4122)

soot. The data for diffusion flames in Fig. 3 show, in general, that the $[SO_4^=]$ fog increased as the $[SO_2]$ was increased above $[SO_2]_{BKGD}$. $[SO_2]_{BKGD}$ is the $[SO_2]$ that was present in the system due to combustion of sulfur in the fuel. $[SO_2]_{BKGD}$ was always less than 0.05 ppm.

A large amount of scatter is associated with the diffusion flame data points in Fig. 3. It was thought that much of the scatter was due to variable soot particle concentrations that occurred from run to run because of irreproducible flame conditions. Normalization of $[SO_4^=]$ to [C] did not significantly reduce the scatter. Other uncontrolled factors could have caused the scatter. Since wet soot particles readily oxidized SO_2 to sulfate, while wet premixed flame particles showed decreased ability to oxidize SO_2, the importance of soot in the droplets was realized. It is not known at this time whether or not a constant fraction of particles becomes covered with water in the condensation process. Visual observations using the laser beam indicated that fogs formed in air streams having soot number concentrations of ~300,000/cm^3 are about as optically dense as fogs formed in air streams having 30,000/cm^2. This suggests that the fraction of the soot particles which becomes wet is variable. It is also not known if the absolute number of droplets which is formed remains constant for a given set of fog generator conditions, regardless of the number of soot particles present. If the number concentration of fog droplets were nearly constant from run to run, more soot particles would be incorporated into fog droplets where the soot concentration is high. This is because the coagulation of soot particles with fog droplets increases as the soot particle concentration increases.

Figure 3 also presents results from experimental runs in which combustion particles from premixed flames were used to nucleate fog droplets. The curve labeled "premixed" in Fig. 3 shows that the $[SO_2]$ does not have a large effect on the amount of sulfate produced and, for a fixed $[SO_2]$, fog droplets which contain premixed flame particles produce little sulfate compared to fog droplets which contain soot particles. The data for the premixed flame curve show little scatter, which tends to confirm the lack of reactivity of wet premixed flame particles.

The particulate carbon concentration for the premixed flame data points was considerably less (as much as a factor of 10) than the runs using soot particles because the premix flames burn much cleaner. The total number concentration of particles produced by the diffusion or premixed flames was not measured routinely but several samples showed that the number concentrations were similar in each. Two L/min of gas was burned in all experimental runs regardless of the flame type, so in terms of sulfate formed per Btu of fuel, the wet soot particles produced the most sulfate.

At this time not enough data are available to determine the shape of the curve for diffusion flame data points in Fig. 3. It is not known whether the $[SO_4^=]$ increases linearly with $[SO_2]$ or whether the curve will gradually level off at high SO_2 concentrations. Evidence from other investigations in our laboratory shows that the rate of sulfite to sulfate oxidation in aqueous soot suspensions, for a constant [soot], increases as the $[SO_3^=]$ increases over several decades of concentration to ~10^{-5} M $SO_3^=$ and above 10^{-5} M $SO_3^=$ the rate remains nearly constant.[9] More data need to be collected before we can determine a rate expression for the fog chamber data.

Rough conversion rate estimates can be calculated from the data in Fig. 3. Such estimates are risky because of the scatter associated with the data. The influence of the soot particle concentration is not taken into account in these estimates because of the difficulty in estimating the "wet" soot particle concentration. For wet soot particles exposed to 10 ppm SO_2, Fig. 3 indicates that approximately 40 μg $SO_4^=/m^3$ can be expected to form in 15 min. This corresponds to a conversion rate of ~0.8%/hr. At an SO_2 concentration of 0.5 ppm, a value of 15 μg $SO_4^=/m^3 \cdot 15$ min was chosen from Fig. 3. This corresponds to a conversion of ~5%/hr which is quite competitive with other mechanisms suggested for sulfate formation in the atmosphere.

CONCLUSIONS

The preliminary results presented here indicate that water can condense onto soot particles and encapsulate them with a liquid layer. Depending on conditions, it is possible that not all the soot particles become encapsulated with water. The

presence of soot in the soot-fog-SO_2 system is important for sulfate formation because experiments conducted with sootless flames produced little sulfate. In general, the amount of sulfate which formed in fog-soot-SO_2 reactions was dependent upon [SO_2] because more sulfate formed at higher SO_2 concentrations.

REFERENCES

1. G. E. Likens, R. F. Wright, J. N. Galloway, and T. J. Butler, "Acid rain," Scientific American 241 (1979).

2. S. A. Penkett, B. M. R. Jones, K. A. Brice, and A. E. J. Eggleton, "The importance of atmospheric ozone and hydrogen peroxide in oxidizing sulphur dioxide in cloud rainwater," Atmos. Environ. 13, p. 123 (1979).

3. G. T. Wolff, P. R. Monson, and M. A. Ferman, "On the nature of the diurnal variation of sulfates at rural sites in the eastern United States," Environ. Sci. and Technol. 13, p. 1271 (1979).

4. L. Enger and U. Hogstrom, "Dispersion and wet deposition of sulfur from a power plant plume," Atmos. Environ. 13, p. 797 (1979).

5. H. F. Johnstone and A. J. Moll, "Formation of sulfuric acid in fogs," Ind. and Eng. Chem. 52, p. 861 (1960).

6. A. C. Dittenhoefer and R. G. de Pena, "A study of production and growth of sulfate particles in plumes from a coal-fired power plant," Atmos. Environ. 12, p. 297 (1978).

7. R. Brodzinsky, S. G. Chang, S. S. Markowitz, and T. Novakov, "Kinetics and mechanism for catalytic oxidation of SO_2 on carbon in aqueous formation," in Atmospheric Aerosol Research Annual Report, 1977-78, Lawrence Berkeley Laboratory Report LBL-8696 (1978).

8. W. H. Benner, H. Rosen, and T. Novakov, "SO_2 oxidation by water droplets containing combustion nuclei," in Atmospheric Aerosol Research Annual Report, 1977-78, Lawrence Berkeley Laboratory Report LBL-8696 (1978).

9. R. Brodzinsky, this year's annual report.

LIFETIME OF LIQUID WATER DROPLETS: AN EXPERIMENTAL STUDY OF THE ROLE OF SURFACTANTS

R. Toossi, et al.

INTRODUCTION

Chemical reactions of air pollutants in liquid water have been extensively studied in the laboratory. These wet processes are suggested to be important in the formation of atmospheric sulfate and nitrate particulates, and thus presumably contribute to the increase in the acidity of rain. The assessment of the impact of wet chemical processes, however, has been largely based on the chemical reaction rates. The effect of the diffusion rate and the lifetime of water droplets has been largely ignored or based on theoretical considerations at best. The experimental measurement of these effects with actual atmospheric water droplets has not been carried out to the best of our knowledge.

Recent studies of atmospheric liquid water droplets[1-3] indicate the presence of various soluble and insoluble impurities. These impurities can drastically affect the evaporation rate of the droplets either by reducing the vapor pressure due to a solution effect or by increasing the surface resistance due to a film of surfactants. For example, a reduction of four orders of magnitude has been observed with a film of certain surfactants.[4] A recent mathematical model[5] shows that the resistance due to surface film can be rate controlling for small droplets ($r << 10$ μm) and small accommodation coefficient ($\alpha < 10^{-4}$). For this reason the accommodation coefficient is an important parameter in studies of water droplet stability.

In this article, we report experimental measurements of the lifetime of water droplets in the presence of various realistic organic impurities which are generated from combustion sources. These results are compared to laboratory-generated fog samples and rain samples. From these measurements, the accommodation coefficients of the various samples are calculated. The measurements will be extended to atmospheric fog and cloud samples in the near future.

EXPERIMENTAL METHODS

Solution droplets were suspended from a quartz fiber located in a quartz spring microbalance. The quartz fiber was coated with a layer of paraffin wax to prevent the droplet from being wetted. Deflections of .001 cm could be measured using a horizontal microscope (magnification of 50x) with an ocular scale. A spring sensitivity of 1 mg/cm allowed the measurement of droplet weight loss with an accuracy of .001 mg. The system was sealed, except for a small leak to equilibrate pressure. The relative humidity in the chamber was maintained with a known concentration of a NaCl solution. A dewpoint hygrometer directly measured humidity in the chamber. This assembly was placed in a thermostatted room where temperature never changed

by more than .2°C during each experiment. A high-intensity lamp was used to illuminate the droplet during each measurement. The lamp was on only for a few seconds during the measurement, and therefore heating of the droplet was not expected. To verify this, measurements were repeated without the light source. No change was observed. Enough time was allowed for the system to reach equilibrium before any measurement was made; then droplet size was measured directly by the microscope and calculated from weight measurements. Referring to Fig. 1, the diameter of the droplet can be calculated from the following formula:

$$m = \frac{1}{6}\pi d^3 - \frac{1}{4}\pi d \cdot d'^2 \quad . \qquad (1)$$

The two methods for determining the diameter of the droplet agreed to within 5%. No attempt was made to measure droplet temperature. Evaporation measurements were made for as long as the droplet remained spherical, usually at one-fifth its original diameter. Experiments have been carried out on a number of laboratory and field samples.

Sample extracts were made by extracting the particulates collected on quartz filters from various combustion-dominated sources such as a tunnel and a parking garage and from ambient samples. Particulates were washed off by sonicating the sample filters in water and then filtering the emulsion to remove large particles. The concentrations of contaminants are normalized by their carbon content determined by a combustion technique. Laboratory fog was collected from a fog chamber which is described in this report (see Benner et al.). The procedure for collection involved impaction on a porous surface and suction by capillary action.

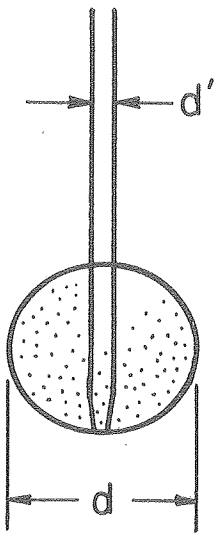

Fig. 1. Schematic drawing of a droplet on a fiber support. d' is the fiber diameter and d is the droplet diameter. (XBL 807-3460)

RESULTS AND DISCUSSION

The equation for the rate of evaporation has been derived as follows:[5]

$$\frac{dr}{dt} = \frac{\rho_{eq}(\infty)}{\rho_\ell} \; \frac{S - (1 - X_s)\exp(2\sigma\rho_{eq}(\infty)/r\rho_\ell)}{R_i + R_m + R_T}$$

where $R_i = \frac{1}{\nu\alpha}$, the resistance at the interface;

R_m is the resistance to mass diffusion;

R_T is the resistance to heat diffusion;

α = the accommodation coefficient;

$\nu = \frac{\bar{v}}{4}$, and $\bar{v}$ is the velocity of the evaporating molecule calculated from the kinetic theory of gases.

$\rho_{eq}(\infty)$ is the equilibrium vapor density at large distances from the droplet, ρ_ℓ is the density of the liquid phase, S is the relative humidity, σ is surface tension, and X_s is mole fraction of solute in the solution droplet. For droplets of 1.0 μm in diameter at 90% relative humidity, only 1% error is introduced when the curvature effect is neglected. With a larger droplet or at a lower humidity, the effect is still smaller. Calculations indicate that the solution effects can be neglected for relative humidities below 70%. The specific rate of evaporation of large droplets of salt solutions (X_s = .01) is only 3.4% lower than those of pure water at S = .70.

The surface degradation rate (- dA/dt) as a function of the accommodation coefficient has been calculated and is plotted in Fig. 2 at different relative humidities. These plots can be used to evaluate the accommodation coefficient of the contaminated droplets if the surface degradation rate is measured experimentally. For pure water, evaporation is controlled by the rate of diffusion, and

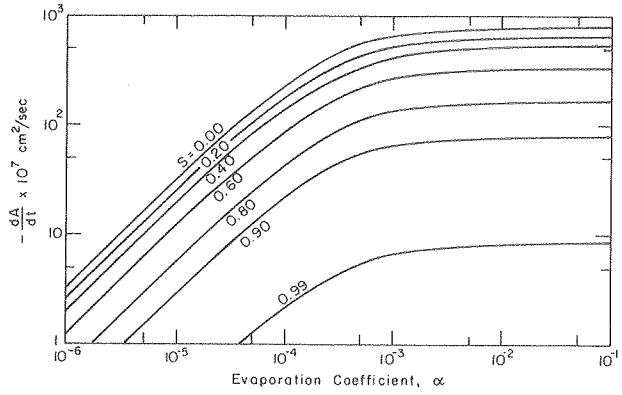

Fig. 2. Surface degradation rate of aerosol droplets. (XBL 801-4500)

the surface degradation rate becomes independent of the accommodation coefficients. Therefore the values of α for pure water cannot be accurately measured by this method. Table 1 gives the measured values of dA/dt for pure water at different relative humidities.

Table 1. Surface degradation rates for pure water.

Relative Humidity	$-\frac{dA}{dt} \times 10^6$ cm^2·sec^{-1}
91	0.320
75	0.766
42	1.710

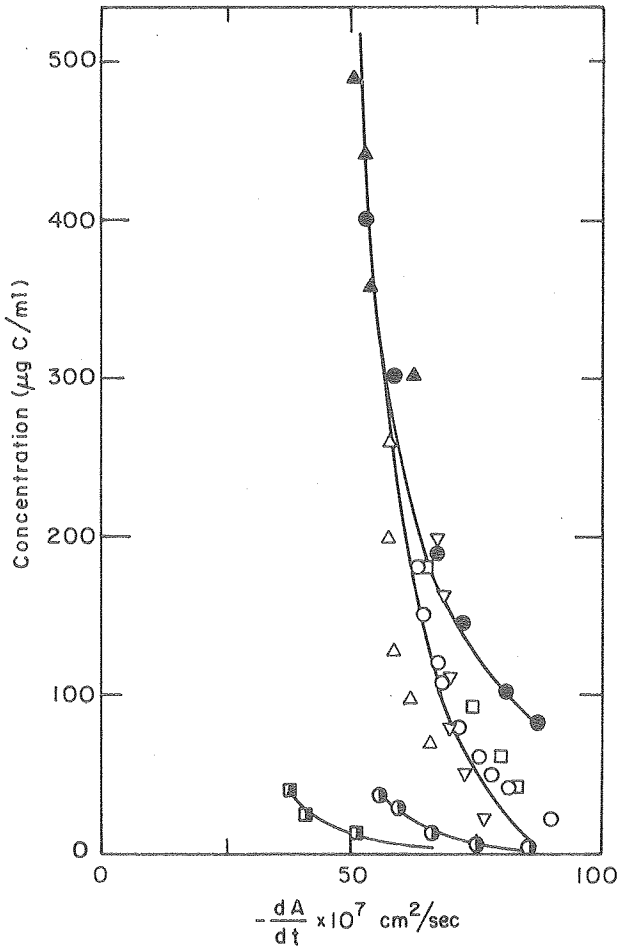

Fig. 3. Surface degradation rate of water extracts of ambient Berkeley and Berkeley rain samples.

△ □ ○ Ambient Berkeley, 3-4 October 1978

▲ ● Ambient Berkeley, 2-3 May 1978

◑ Berkeley rain, 24-27 March 1978

◨ Berkeley rain, 6 April 1978

Different symbols on the same graph represent results for different samples prepared at different initial contaminant concentrations from the same extract. (XBL 801-4505)

However, for sufficiently contaminated drops the evaporation coefficient can be found from the surface degradation rate curves. Figures 3 and 4 show such graphs for rain and water extract of ambient Berkeley particulate aerosol samples. Results from tunnel samples, parking garage samples, and laboratory fog are shown in Fig. 5. These figures show that there exists a critical concentration of contaminants, above which evaporation is greatly retarded. At this concentration a monolayer of surfactant presumably covers the entire droplet surface. All molecules of water vapor have to cross this barrier before evaporating into gaseous media. At lower concentrations all the sites are not filled, and water molecules can bypass this resistance. Therefore evaporation is controlled by diffusion and proceeds like pure water until the solution becomes concentrated enough for the solution effect to become important.

A summary of these results is given in Table 2. The lifetimes of droplets of 10 μm in diameter are estimated at relative humidities of 60% and 90% where the surfactant concentration is greater than the critical concentration. A comparison of these results with those of pure water, which is also shown in the table, indicates that surfactants if present in sufficient quantities can have a large effect on the lifetime of liquid water drops in the atmosphere.

REFERENCES

1. D. Winkler and C. Junge, "The growth of atmospheric aerosol particles as a function of the relative humidity. Part II. An improved concept of mixed nuclei," Aerosol Sci. 4, 373 (1973).

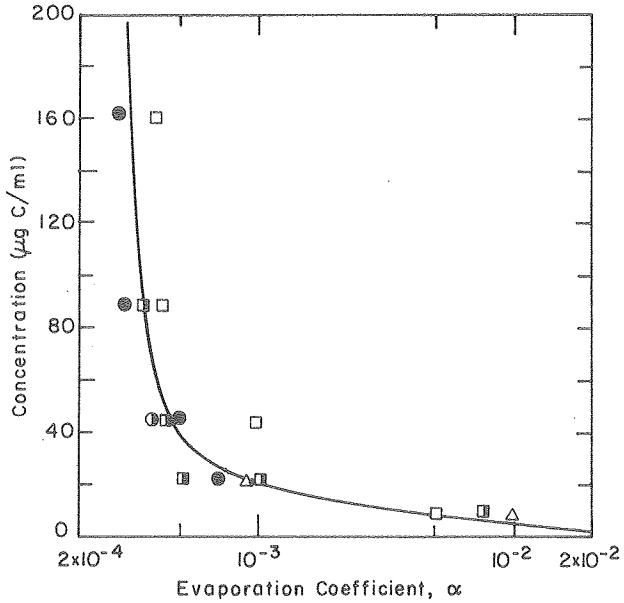

Fig. 4. Evaporation coefficient for water extract of an ambient Berkeley sample as a function of the carbon content. (XBL 801-4504)

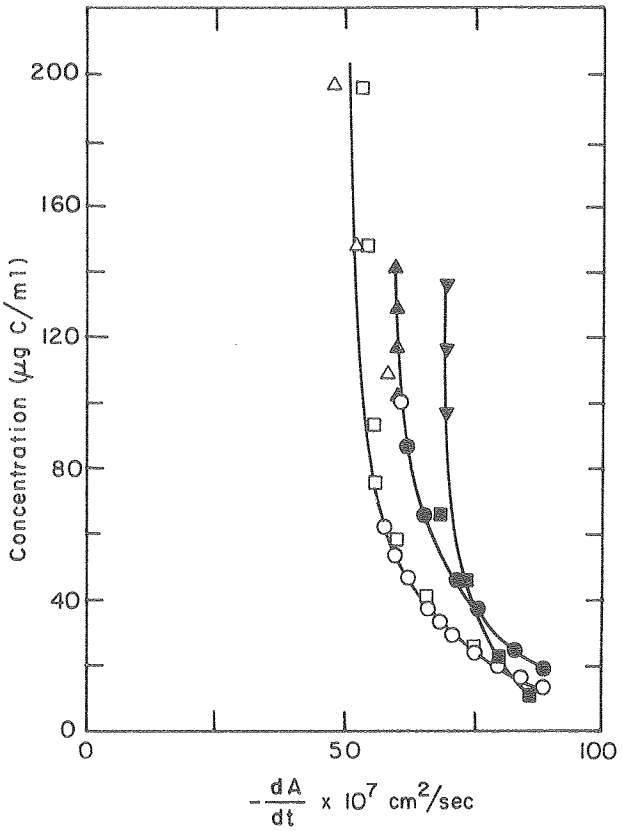

Fig. 5. Evaporation coefficient for water extract of an ambient Berkeley sample as a function of the carbon content. (XBL 801-4503)

Table 2. Evaporation coefficients and associated lifetimes of different aerosol samples.

Sample	Date collected	α	Lifetime (minutes) r_o = 5 μm S = .60	S = .90
Ambient Berkeley	10/3-4/78	7×10^{-5}	1.5	10
	5/2-3/78	7×10^{-5}	1.5	10
Tunnel	3/30/78	7×10^{-5}	1.5	10
	3/30/78	10^{-4}	0.7	4
Parking garage	4/14/78	6×10^{-5}	2.0	12
	4/15/78	6×10^{-5}	2.0	12
Laboratory fog	11/1/79	1.4×10^{-4}	0.4	2
Pure water	--	4×10^{-2} [a]	$<10^{-2}$	10^{-2}

[a] Ref. 6.

2. D. S. Covert, "A study of the relationship of chemical composition and humidity to light scattering by aerosols," J. Appl. Meteorol. 11, 968 (1972).
3. Yu. S. Georgievskiy and G. V. Rosenberg, "Humidity as a factor in aerosol variability," Izv. Atmos. Oceanic Phys. 9, 66 (1973).
4. R. S. Bradley, "The rate of evaporation of micro-drops in the presence of insoluble monolayers," J. Coll. Sci. 10, 751 (1955).
5. R. Toossi, S. G. Chang, and T. Novakov, "Lifetime of liquid water drops in ambient air: Consideration of the effects of surfactants and chemical reactions," in Atmospheric Aerosol Research Annual Report, 1977-78, Lawrence Berkeley Laboratory Report LBL-8696 (1978).
6. N. A. Fuchs, Evaporation and Droplet Growth in Gaseous Media (English translation), New York, Pergamon (1959).

A PHOTOACOUSTIC INVESTIGATION OF URBAN AEROSOL PARTICLES*

Z. Yasa, et al.

INTRODUCTION

The nature of the absorbing species in atmospheric aerosol particles has recently attracted considerable attention among atmospheric and environmental scientists. Recent studies using Raman spectroscopy and an optical attenuation technique[1] indicate that the absorbing species in urban particulates is "graphitic" carbon. We report here on the results of a photoacoustic investigation which gives an independent verification of this hypothesis.

Unlike conventional optical absorption techniques, photoacoustic spectroscopy measures the energy deposited in a sample due to absorption. Since questions have been raised whether the optical attenuation technique exclusively measures the absorbing rather than the scattering component of the aerosol, a comparison between photoacoustic and optical attenuation measurements made on the same aerosol sample should help resolve this ambiguity.

EXPERIMENTAL METHOD AND RESULTS

The photoacoustic measurements were made in an acoustically nonresonant detector with cylindrical geometry (Fig. 1). A Knowles microphone (Model BT-1759) was used, and the cell dimensions were 2.1 cm in diameter and 0.3 cm in length. The gas in the detector cell was air at atmospheric pressure. A He-Ne laser operating at 632.8 nm with 0.5 mW of power was used as the light source, and the experiments were performed at a modulation frequency of 20 Hz. The aerosol particles, collected on 1.2-μ Millipore filter substrates, were mounted on a 1.5-mm-thick Pyrex backing with the particles facing the incident light beam. Experiments were also performed with the laser beam first incident on the filter substrate.

In the limit of low frequency light modulation ($\leq$100 Hz), it can be shown[2,3] that the photoacoustic signal is given by:

$$V(\omega) = \frac{\eta\gamma PW\mu_g\mu_{sb}G(\omega)}{2\sqrt{2}bTVK_{sb}} \quad 1-\exp(-\alpha\ell) \qquad (1)$$

where η - heat conversion efficiency

γ - specific heat ratio for air (Cp/Cv)

P - cell pressure

W - input power

μ_g - thermal diffusion length in air

μ_{sb} - thermal diffusion length in substrate

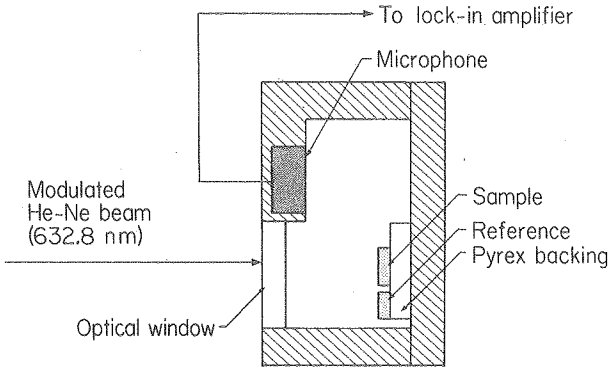

Fig. 1. Experimental arrangement. (XBL 794-1230)

$G(\omega)$ - microphone response

b - dimensionless parameter taking into account the diffusion of heat from the sample to the Pyrex backing

T - temperature

V - cell volume

K_{sb} - thermal conductivity of substrate

α - adsorption coefficient

ℓ - effective path length .

From Eq. (1) it follows that the photoacoustic signal saturates exponentially with increasing absorption to a value of

$$V_{sat}(\omega) = \frac{PW\mu_g\mu_{sb}G(\omega)}{2\sqrt{2}bTVK_{sb}} \quad . \qquad (2)$$

Hence the ratio of the signal from a given sample to a reference sample for which the signal is saturated yields

$$S_{ph} = V/V_{sat} = 1-\exp(-\alpha\ell) \quad . \qquad (3)$$

This saturable behavior was observed for highly absorbing samples, and the sample which yielded the largest photoacoustic signal was used as the reference, V_{sat}. Note that such samples yield values of $\alpha\ell \geq 3$, as deduced from the optical attenuation measurements; hence the highest signal obtained from available samples is close to the actual saturation value.

The experimental setup for the optical attenuation measurements is described elsewhere.[1] In this technique the signal S_{op} is defined as $1-\exp(-x)$. x is the optical attenuation of the sample and is given by $-\ln I/I_0$, where I is the transmitted intensity of a loaded filter, and I_0 is the transmitted intensity of a blank filter.

In Fig. 2 we present a plot of the normalized photoacoustic signal S_{ph} vs. S_{op} for a wide range of ambient samples and samples collected directly from combustion sources. The samples include urban particulates collected over a 24-hr period in Fremont and Anaheim, California; Denver, Colorado; and New York, New York; particles collected in a highway tunnel and from an acetylene torch. The least squares fit of the experimental points yields a correlation coefficient r of 0.98 and a slope of 1.03, which would be expected if both techniques measure the same optical property of the aerosol particles. Since the photoacoustic signal is proportional to the heat generated by absorption, we conclude that the optical attenuation method measures the light absorbing component of the aerosol particles.

From a theoretical point of view, this result is somewhat surprising since aerosol particles have a large scattering coefficient, which would be expected to contribute to the optical attenuation measurement and not to the photoacoustic signal. However, careful examination of the experimental arrangement shows that the incident light interacts not only with the aerosol particles but also with the filter medium, which is almost a perfect diffuse reflector. In this circumstance, it is possible to show[4] that because of multiple reflections between the particles and the filter substrate, the optical attenuation measurement is insensitive to the scattering properties of the aerosol.

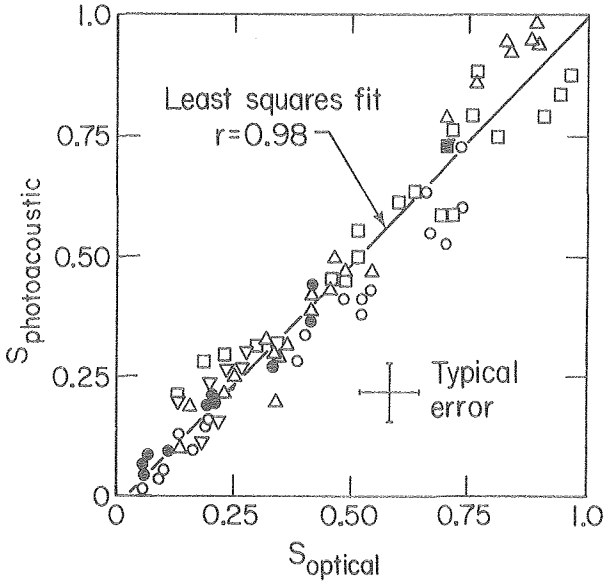

Fig. 2. Plot of S_{ph} vs. S_{op} for various samples: ▽- Fremont; □- Anaheim; ○- Denver; △- New York City; ■- highway tunnel; ●- acetylene torch. The solid line is a least squares fit of the data. (XBL 794-1229)

CONCLUSION

In conclusion, the results presented here, when combined with Raman scattering data[1] and thermal analysis[5] and solvent extraction results,[6] indicate that the optically absorbing component of urban aerosol particles is "graphitic" carbon. Extensions of this work are presently being carried out in our laboratories.

FOOTNOTE AND REFERENCES

*Collaborative work between Applied Laser Spectroscopy group and Atmospheric Aerosol Research group. (Published in Applied Optics 18, 2528 (1979).

1. H. Rosen, A. D. A. Hansen, L. Gundel, and T. Novakov, "Identification of the optically absorbing component in urban aerosols," Appl. Opt. 17, 3859 (1978).

2. Over a frequency range of 5-100 Hz, the photoacoustic signal showed no variation, indicating that the sample was thermally thin. In this case Eq. (1) follows from Eq. (21) of Ref. 3 in the limit of $\omega \to 0$ and after modification of their parameters to take into account an additional boundary layer introduced by the Millipore filter.

3. A. Rosenzwaig and A. Gersho, "Theory of photoacoustic effect with solids," J. Appl. Phys. 47, 64 (1976).

4. H. Rosen and T. Novakov, "Optical attenuation: a measurement of the absorbing properties of aerosol particles," in Atmospheric Aerosol Research Annual Report 1977-78, Lawrence Berkeley Laboratory Report LBL-8696, p. 54.

5. H. Rosen, A. D. A. Hansen, L. Gundel, and T. Novakov, "Identification of the graphitic carbon component of source and ambient particulates by Raman spectroscopy and an optical attenuation technique," Proceedings of Conference on Carbonaceous Particles in the Atmosphere, Lawrence Berkeley Laboratory Report LBL-9037 (1979).

6. R. E. Weiss, A. P. Waggoner, R. J. Charlson, D. L. Thorsell, J. S. Hall, and L. A. Riley, "Studies of the optical, physical, and chemical properties of light absorbing aerosols," Proceedings of Conference on Carbonaceous Particles in the Atmosphere, Lawrence Berkeley Laboratory Report LBL-9037 (1979).

THE USE OF AN OPTICAL ATTENUATION TECHNIQUE TO ESTIMATE THE CARBONACEOUS COMPONENT OF URBAN AEROSOLS

A. Hansen, et al.

INTRODUCTION

Carbon-, sulfur-, and nitrogen-containing particles account for most of the anthropogenically generated particulate burden in urban areas. The carbonaceous aerosol is often the single most important contributor to the submicron aerosol mass and is expected to have a substantial impact on visibility and health.[1] It was also postulated as early as 1974[2] that the surface of these particles might be an effective catalyst for the heterogeneous conversion of SO_2 to sulfate in the presence of moisture--a process that has subsequently been confirmed both theoretically[3] and under laboratory conditions.[4,5] These carbonaceous particles consist of two major components--graphitic or black carbon (sometimes referred to as elemental or free carbon) and organic material. The latter can either be directly emitted from sources (primary organics) or produced by atmospheric reactions from gaseous precursors (secondary organics). We define "soot" as the total primary carbonaceous material, i.e., the sum of graphitic carbon and primary organics. There has been considerable uncertainty and debate over the relative importance of primary and secondary carbonaceous material in urban air.[1] It is important to resolve this issue since it is obvious that a control strategy and technology for particulate carbon pollution abatement will depend on which of these alternatives prevails. In this paper we present data from a large-scale sampling program and results showing that a measurement of the optical absorption of the particles may be used to quantitate the black carbon component and to estimate the total carbon loading.

SAMPLING AND EXPERIMENTAL METHODS

Because relatively few consistent studies of ambient carbonaceous particles had been conducted, we established in 1977 an ongoing routine sampling program at numerous sites. The data consist of information obtained from 24-hour samples (collected every morning Monday through Friday) and multi-day samples collected over weekends. For the purpose of data analysis, these two data sets can be separated. Table 1 lists the routine sampling sites with the beginning date of sampling.

The samples are collected in parallel on prefired quartz fiber and Millipore filter membranes. The flow rates employed are in the range of 0.6-2.2 cubic meters of air per square centimeter of active filter area per 24-hour sampling period. The Millipore filter is used for x-ray fluorescence (XRF) elemental analysis and an optical attenuation technique developed in this laboratory.[6] The latter technique gives a measurement that is proportional to the amount of light-absorbing (black) carbon present on the filter.[7] It is based on a principle similar to that of the opal glass method used by Weiss et al.[8] and measures the absorbing rather than the scattering properties of the aerosol. For fixed optical constants, a quantitative relationship between the optical attenuation and the black carbon content can be written as:

Table 1. Aerosol sampling sites.

Site	Location	Date of first sample
Lawrence Berkeley Laboratory	Berkeley, Calif.	1 June 1977
BAAQMD monitoring station	Fremont, Calif.	15 July 1977
SCAQMD monitoring station	Anaheim, Calif.	19 August 1977
Argonne National Laboratory	Argonne, Ill.	22 January 1979
DOE Environmental Measurements Laboratory	Manhattan, New York	22 November 1978
National Bureau of Standards	Gaithersburg, Maryland	23 January 1979
Denver Research Institute	Denver, Colorado	15 November 1978
Naval Arctic Research Station	Barrow, Alaska	1 October 1979
Oregon Graduate Center	Beaverton, Oregon	22 April 1979
University of Arizona	Tucson, Arizona	8 March 1979
University of Washington	Seattle, Washington	14 February 1979
C.S.I.R.O.	Sydney, Australia	11 September 1978
B. Kidric Institute	Belgrade, Yugoslavia	1 October 1979
National Center for Atmospheric Research	Boulder, Colorado	4 January 1980

The latter six samplers have been operated on an intermittent basis. In addition to the above locations, samplers are currently being shipped to the following locations:

Cheng Kung University, Taiwan, Republic of China
Washington University, St. Louis, Missouri

$$[C_{black}] = (1/K) \times ATN \quad , \qquad (1)$$

where $ATN = -100 \ln(I/I_0)$. I and I_0 are the transmitted light intensities for the loaded filter and for the filter blank.

Besides the black carbon, particulate material also contains organic material which is not strongly optically absorbing. The total amount of particulate carbon is then:

$$[C_{tot}] = [C_{black}] + [C_{org}] \ . \qquad (2)$$

A fundamental characterizaion of a particulate sample can be given by its attenuation per unit mass of total carbon, i.e., its specific attenuation, σ:

$$\sigma \equiv \frac{ATN}{[C_{tot}]} = K \times [C_{black}]/[C_{tot}] \ . \qquad (3)$$

The determination of specific attenuation therefore gives an estimate of black carbon as a fraction of total carbon.

Carbon-specific analyses are performed on the quartz fiber filter, since the carbon loading of a blank is typically 30 to 100 times less than the loading after exposure. These analyses include total combustible carbon determination,[9] successive solvent extraction[10] to separate nonextractable and "organic" carbonaceous material, and a progressive combustion-optical attenuation technique[11] that yields both chemical and physical information. The information recorded in the data base includes the above particulate analyses as well as meteorological and gaseous pollutant data and may be used in many ways to study seasonal effects and intercorrelation of pollutants. In this report we concentrate on studies of the concentration of "total" and "black" carbon in the ambient aerosol.

Total Carbon Loadings

From analysis of the quartz fiber filters, we may determine the average loading of particulate carbonaceous material during the sampling period. Overall average carbon concentrations are shown in Table 2. In Fig. 1 we show the variations of total carbon at the Fremont site for 24-hour samples (i.e., weekends excluded), with the monthly averages superimposed. It is evident that there are large day-to-day variations, but that the averages peak during the late fall season. A similar pattern is observed at other California locations, supporting the hypothesis that the loadings at these receptor sites are largely controlled by ventilation. In contrast, results from the New York site (Fig. 2) show much less variation on both a daily and monthly scale. This is consistent with the location of the site above a heavily traveled street canyon, resulting in an aerosol dominated by direct source emissions.

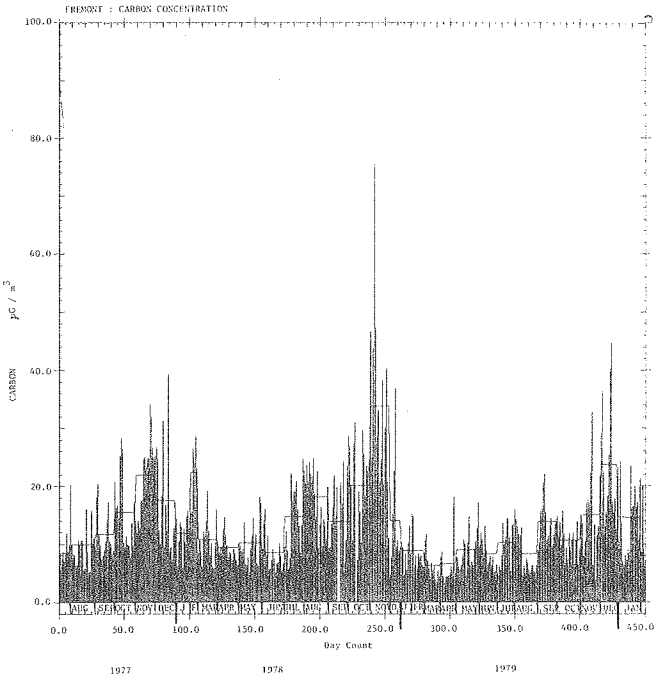

Fig. 1. Total carbon loading of 24-hour samples taken at the Fremont site. (XBL 806-10534)

From XRF analysis of the Millipore filter we obtain the loadings of silicon and heavier elements. We may apply a simple model of the chemical form of these elements to calculate an "accountable mass" from this data. The algorithm used is necessarily crude and overlooks important contributions of oxygen and nitrogen. Reported figures for the mass contribution of water to the accumulation

Table 2. Carbon concentrations ($\mu g/m^3$)

Site	Dates on file	# samples	Average	Highest	Lowest
New York	Nov. 78 - Apr. 80	439	15.2	53.1	3.4
Argonne	Jan. 79 - Mar. 80	438	8.1	25.1	3.1
Gaithersburg	Jan. 79 - Mar. 80	381	6.1	17.6	2.3
Denver	Nov. 78 - May 79	141	9.8	30.8	4.1
Anaheim	Aug. 77 - Jan. 80	852	16.6	112.9	3.1
Fremont	July 77 - Mar. 80	924	12.0	75.6	3.4
Berkeley	June 77 - Apr. 80	998	6.7	31.7	3.0

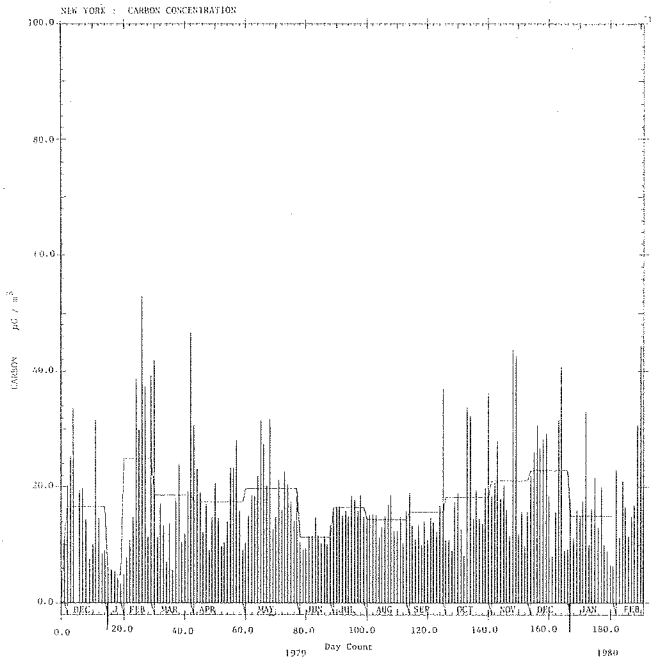

Fig. 2. Total carbon loading of 24-hour samples taken at the New York City site.
(XBL 806-10535)

mode of ambient aerosols range up to 20%,[12] and loadings of up to 30 $\mu g/m^3$ of nitrate are not uncommon.[13] The conventional nitrate determination method has been subject to question on the basis of artifact formation,[14] but may still be indicative of substantial quantities.

Despite these obvious sources of underestimation, we find a good correlation ($r > 0.8$ in all cases) between particulate carbon and accountable mass at all locations, with a proportionality, representing the percentage contribution of carbon, that varies widely as shown in Table 3.

At present the best interpretation of these results is that the Denver aerosol probably consists mainly of carbon, oxygen, nitrogen, and hydrogen, while the Washington aerosol contains a large contribution of other elements, notably sulfur and silicon. Note that the two most polluted locations, Anaheim and New York, both have a 40-50% contribution of particulate carbon to the accountable mass.

Data on actual total suspended particulate mass are available at some sites for a fraction of the number of days sampled. We find a good correlation at the Fremont and Anaheim locations between TSP measurements and our calculated "accountable mass," with similar proportionality at the two sites and similarity between heavily loaded and clean days. These facts suggest a roughly constant aerosol composition.

Table 3. Average percentage of carbon in calculated accountable mass.

Berkeley	55%	Chicago	37%
Fremont	48%	New York	49%
Anaheim	41%	Washington	28%
Denver	83%		

"Black" Carbon

The carbonaceous fraction of the aerosol is a complex mixture of many forms and compounds of carbon. Solvent extraction is capable of characterizing this material into the categories of "polar extractable," "nonpolar extractable," and "nonextractable." Generally we find about 35% (±10%) of the carbonaceous material to be nonextractable for California ambient samples, rising to about 55% (±10%) for samples from New York. In nearly all cases we find that the optical attenuation of a filter is affected very little by solvent extraction, as shown in Fig. 3. This suggests that the material responsible for the optical absorption is nonextractable carbon that may have a "graphitic"-like form. This form of carbon would be expected to be relatively stable in oxygen at elevated temperatures, a hypothesis that is validated by the progressive thermal analysis method. From this latter method we generally find that the optical attenuation remains until temperatures of around 450°C, at which the rate of removal of optical attenuation is often closely followed by the rate of CO_2 detection (see Fig. 4). A comparison of the room-temperature optical attenuation measurement with the amount of carbon represented by the area under the high-temperature peak in the CO_2 evolution curve is shown in Fig. 5. In Fig. 6 we show the optical attenuation versus the amount of nonextractable carbon; both these figures contain data from a variety of ambient samples as well as source emission samples. In each figure a line is drawn representing a specific attenuation of 20. We see that many of the thermogram points lie a little above this line, a feature that would be accentuated by incomplete recovery of the carbon as CO_2 after combustion. On the other hand, the extraction data often lie below the line,

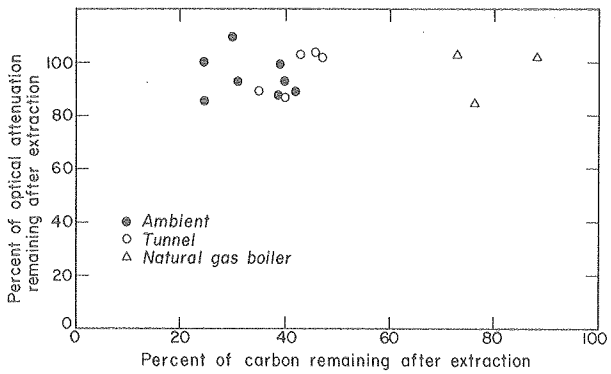

Fig. 3. Plot of the percent of the optical attenuation remaining after successive Soxhlet extraction in benzene and a methanol-chloroform mixture as a function of the carbon remaining after extraction for various ambient and source particulate samples.
(XBL 783-344)

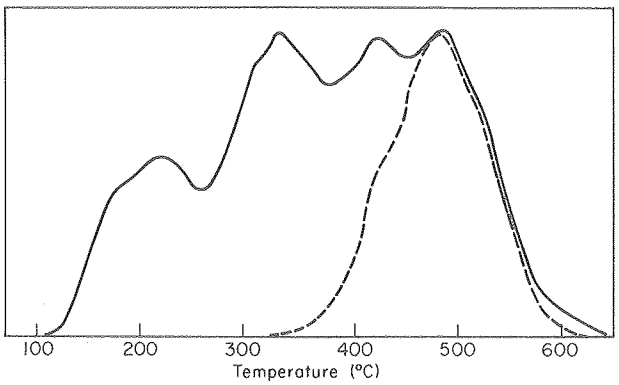

Fig. 4. Progressive thermal analysis result on ambient sample from Sydney, Australia. Solid curve - rate of CO_2 detection. Dashed curve - rate of change of optical attenuation. (Arbitrary units, scaled to match). (XBL 807-3461)

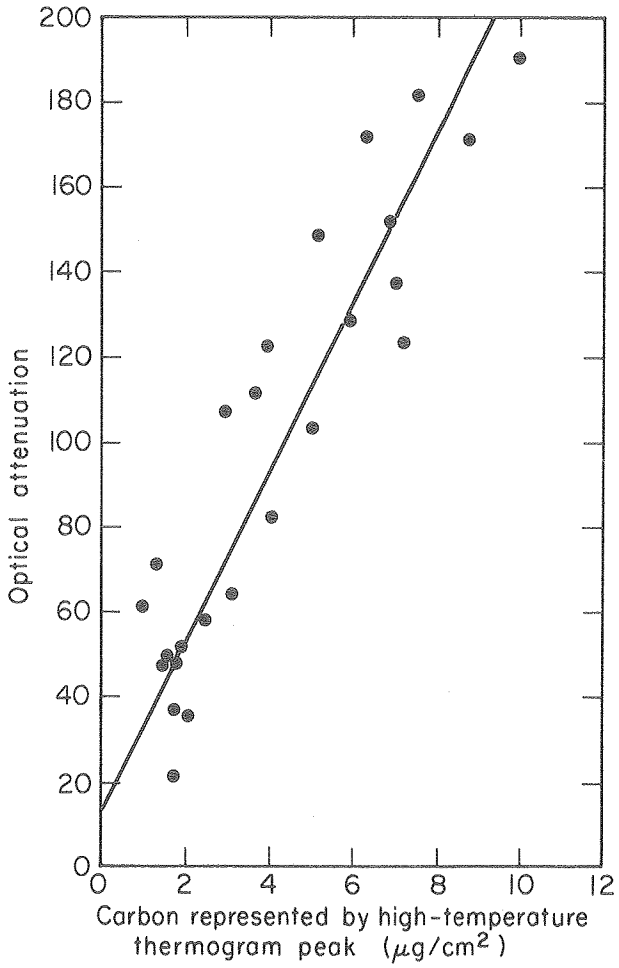

Fig. 5. Graph of optical attenuation versus carbon represented by high-temperature thermogram peak. Line is best fit to points. (XBL 807-3462)

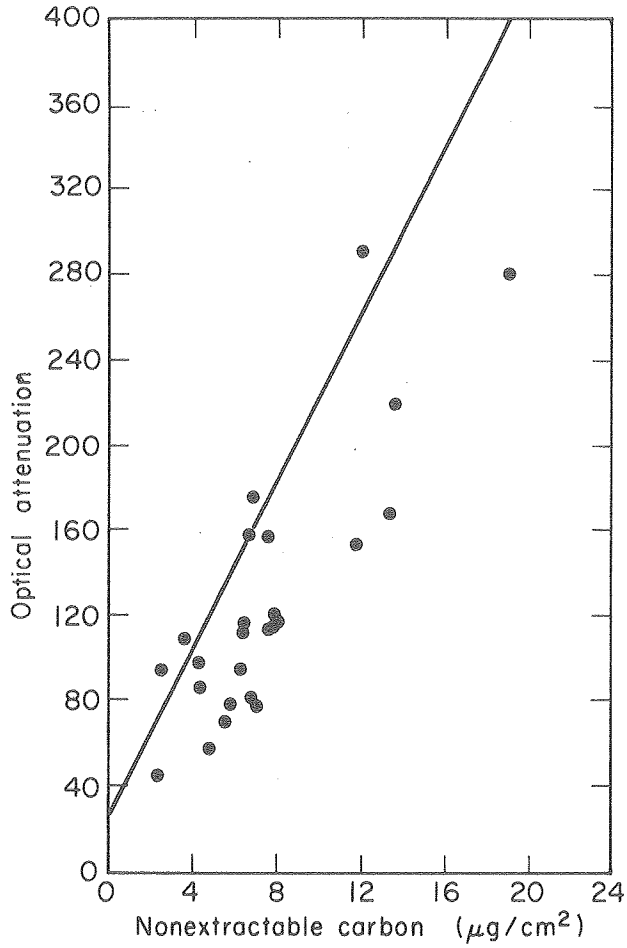

Fig. 6. Graph of optical attenuation versus nonextractable carbon. Line is best fit to Fig. 5. (XBL 807-3463)

possibly characteristic of incomplete extraction. The line $\sigma = 20$ is the basis of our operational definition of "black" carbon. Black carbon is that fraction of the carbonaceous aerosol, responsible for optical absorption, that yields a transmission attenuation measurement in our apparatus of 20 units (optical density 0.2 at 6328 Å) when deposited on a Millipore filter with a surface density of 1 $\mu g/cm^2$. It is nonextractable and stable in oxygen for moderate lengths of time at temperatures of up to about 400°C.

Correlations Between Total Carbon and ATN

Statistical analysis of the data shows that there is a strong correlation ($r > 0.85$) between optical attenuation and total particulate carbon at every site studied.[14] Furthermore, a study of a number of source samples shows that there is also a strong correlation between optical attenuation and total carbon for these samples. The correlations between optical attenuation and total carbon for ambient samples and source samples are discussed in the following paper.

Results obtained from ambient samples imply that the fraction of graphitic soot to total particulate carbon is approximately constant under

the wide range of conditions occurring at a given site. On specific days, however, there can be large variations in the ratio, reflecting the variations in the relative amounts of organic and black carbon. The least squares fit of the data shows regional differences which are related to the fraction of black carbon due to primary emissions. These differences would suggest an increase in the relative importance of the primary component for samples collected respectively at Berkeley, Fremont, Anaheim, Argonne, and New York.

Black Carbon in Ambient Aerosols

Figure 7 displays the optical attenuation of 24-hour samples from the Fremont site. The pattern is very similar to that of Fig. 1, representing the total carbon content of those samples. This suggests a roughly constant aerosol composition in terms of the ratio of black to total carbon. Figure 8 shows this ratio, expressed as the specific attenuation [attenuation]/[total carbon]. We may use the value of 20 for the specific attenuation of black carbon to convert the specific attenuation of an ambient sample into a measure of its black carbon content:

$$[BC]/[C] = \sigma_{ambient}/20 \qquad (4)$$

The compositional variations represented in Fig. 8 are much less pronounced than the absolute loadings (Figs. 1,7) and show no clear seasonal pattern. Similar features of total C, ATN, and ATN/C are also observed at the Berkeley and Anaheim sites. At the New York, Gaithersburg, and Argonne sites, daily and monthly variations of total C and ATN are much less pronounced than at the three West Coast sites. The black carbon fractions (ATN/C) values) at these sites also do not show any systematic seasonal trends.

Concentrations of Black Carbon

Determination of specific attenuation, $\sigma \equiv$ ATN/C, enables a straightforward estimation of black carbon. From relation (4) one can calculate black carbon as a percentage of total carbon, and the concentration of black carbon in $\mu g/m^3$. Table 4 lists the average specific attenuation (σ) and black carbon (BC) percentages for all samples (including multi-day samples) analyzed to date. In addition to the average values, the highest and lowest values are given. Based on this estimate, on the average 20% of the total carbon is black carbon. This fraction can on occasion be as high as 56% or as low as 6%. The latter occurs as a rule when total carbon concentrations are low.

CONCLUSIONS

We may summarize the results presented in the previous sections as follows:

1. There are substantial quantities of carbon present in the ambient aerosol at every sampling site studied so far.

2. This carbon contains a black component that may be rapidly quantitated by the optical attenuation measurement.

3. The fact that the black carbon accounts for an approximately constant fraction of the carbonaceous aerosol at all locations

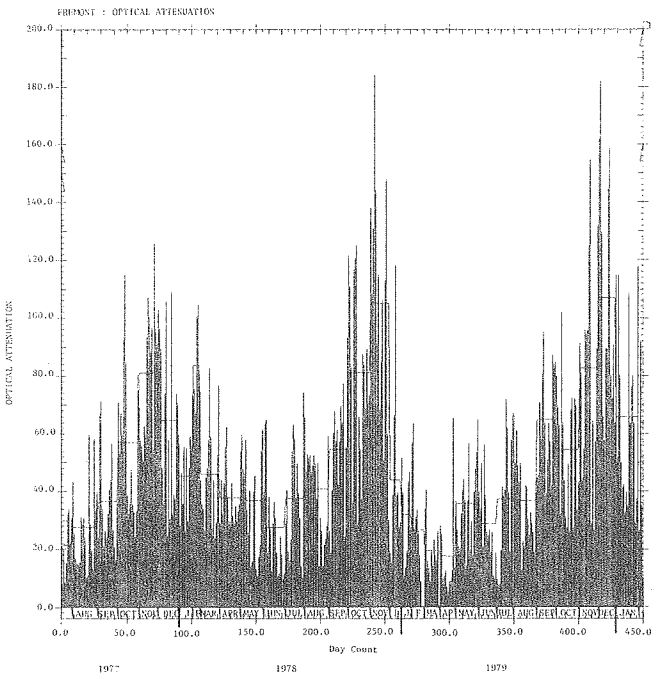

Fig. 7. Optical attenuation of 24-hour samples taken at the Fremont site. (XBL 806-10536)

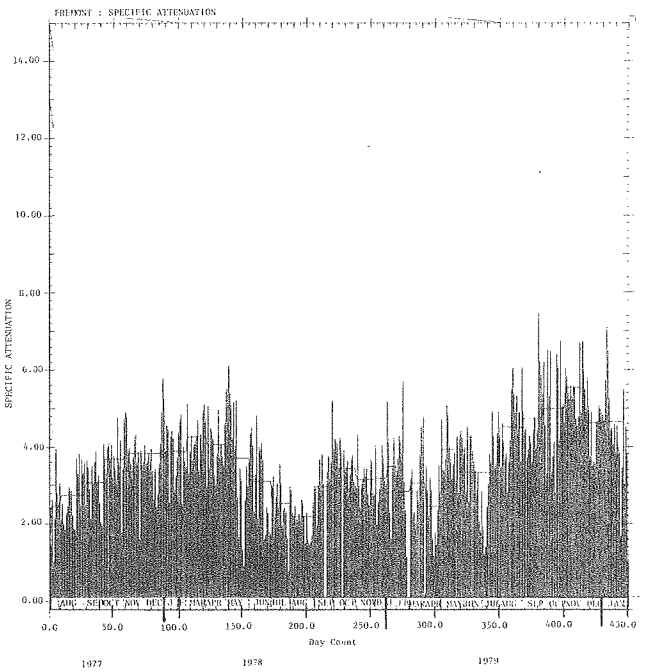

Fig. 8. Specific attenuation of 24-hour samples taken at the Fremont site. (XBL 806-10537)

Table 4. Specific attenuation (σ) and black carbon (BC) (% of total C) from ambient samples.

Site	Average		Highest		Lowest	
	σ	%BC	σ	%BC	σ	%BC
New York	5.44	27%	11.1	56%	2.8	14%
Argonne	4.30	22%	9.1	46%	1.1	6%
Gaithersburg	4.33	22%	8.0	40%	1.8	9%
Denver	3.23	16%	5.7	29%	1.4	7%
Anaheim	3.70	19%	9.6	48%	0.8	4%
Fremont	3.55	18%	8.3	42%	1.6	8%
Berkeley	4.09	20%	9.2	46%	1.2	6%

implies that the optical attenuation measurement may be used to estimate the total carbon content of an ambient sample.

REFERENCES

1. Proceedings, Conference on Carbonaceous Particles in the Atmosphere, T. Novakov, ed., Lawrence Berkeley Laboratory Report LBL-9037 (1979).

2. T. Novakov, S. G. Chang, A. B. Harker, "Sulfates as pollution particulates: Catalytic formation on carbon (soot) particles," Science 186, 259 (1974).

3. R. Toossi, T. Novakov, and S. G. Chang, "Relative importance of various sulfate production mechanisms in aqueous droplets," in Atmospheric Aerosol Research Annual Report, 1977-78, Lawrence Berkeley Laboratory Report LBL-8696 (1978), p. 132.

4. W. H. Benner, H. Rosen, and T. Novakov, "SO_2 oxidation by water droplets containing combustion nuclei," in Atmospheric Aerosol Research Annual Report, 1977-78, Lawrence Berkeley Laboratory Report LBL-8696 (1978), p. 88.

5. R. Brodzinsky, S. G. Chang, S. S. Markowitz, and T. Novakov, "Kinetics and mechanism for the catalytic oxidation of SO_2 on carbon in aqueous suspensions," in Atmospheric Aerosol Research Annual Report, 1977-78, Lawrence Berkeley Laboratory Report LBL-8696 (1978), p. 110.

6. A. D. A. Hansen, H. Rosen, R. L. Dod, and T. Novakov, "Optical characterization of ambient and source particulates," in Proceedings, Conference on Carbonaceous Particles in the Atmosphere, T. Novakov, ed., Lawrence Berkeley Laboratory Report LBL-9037 (1979), p. 116.

7. H. Rosen and T. Novakov, "Optical attenuation: A measurement of the absorbing properties of aerosol particles," in Atmospheric Aerosol Research Annual Report, 1977-78, Lawrence Berkeley Laboratory Report LBL-8696 (1978), P. 54.

8. R. E. Weiss, A. P. Waggoner, R. J. Charlson, D. L. Thorsell, J. S. Hall, and L. A. Riley, in Proceedings, Conference on Carbonaceous Particles in the Atmosphere, Lawrence Berkeley Laboratory Report LBL-9037 (1979).

9. P. K. Mueller, R. W. Mosley, and L. B. Pierce, "Carbonate and noncarbonate carbon in atmospheric particulates," in Proceedings, Second International Clean Air Congress (New York, Academic, 1971).

10. L. A. Gundel, G. E. Mason, and T. Novakov, "Characterization of source and ambient particulate samples by solvent extraction," in Atmospheric Aerosol Research Annual Report, 1977-78, Lawrence Berkeley Laboratory Report LBL-8696 (1978), p. 68, and references therein.

11. R. L. Dod, H. Rosen, and T. Novakov, "Optico-thermal analysis of the carbonaceous fraction of aerosol particles," in Atmospheric Aerosol Research Annual Report, 1977-78, Lawrence Berkeley Laboratory Report LBL-8696 (1978), p. 2.

12. H. Puxbaum, "Die Charakterisierung von Kohlenstoff, Schwefel und Stickstoffverbindungen in luftgetragenen Stauben durch kombinierte thermische und gasanalytische Methoden," submitted to Fresenius Zeit. f. Anal. Chemie.

13. Monitoring data from South Coast Air Quality Management District and Bay Area Air Quality Management District.

14. C. W. Spicer and P. M. Schumacher, "Particulate nitrate: Laboratory and field studies of major sampling interferences," Atmos. Environ. 13, 543 (1979).

IDENTIFICATION OF SOOT IN URBAN ATMOSPHERES BY AN OPTICAL ABSORPTION TECHNIQUE*

H. Rosen, et al.

INTRODUCTION

Particulate carbon is a major fraction of the respirable particulate burden in urban atmospheres, yet the chemical composition and origin of this component are poorly understood. The major cause of these particles is fossil fuel combustion, which produces both primary particulate carbonaceous emissions (soot) and gaseous hydrocarbons, which can be transformed in the atmosphere by gas-to-particle conversion processes to secondary organic material.[1] For an effective control strategy, it is necessary to establish the relative importance of each of these components. In this paper we describe the application of a new method of analysis which uses the unique optical properties of "graphitic"[2] soot to trace the primary component of the carbonaceous particulates under widely different atmospheric conditions over a wide geographical area. The results of our work are consistent with the earlier work of Novakov et al.[3] and indicate that primary soot emissions compose a major fraction of the urban carbonaceous aerosol.

Soot consists of a "graphitic" component and an organic component. The "graphitic" component can be conveniently monitored because of its large and uniform optical absorptivity, which has recently been shown to be responsible for the gray or black appearance of ambient and source particulate samples collected on various filter media.[4-6] The "graphitic" content of the aerosol can be measured by an optical attenuation method developed in our laboratory.[4] In addition to the attenuation, we have also determined total particulate carbon, which enables us to study the correlation between the "graphitic" and the total carbon content of the aerosol.[7] The correlation or lack of it should depend on the relative amounts of primary and secondary material.

EXPERIMENTAL METHODS AND RESULTS

Measurements have been obtained of the optical attenuation and the total carbon content of over 1000 ambient samples collected in two California air basins and in the Chicago area. These samples have been collected daily from 1 June 1977 at Lawrence Berkeley Laboratory, Berkeley, California; from 15 July 1977 at the Bay Area Air Quality Management District monitoring station, Fremont, California; and from 19 August 1977 at the South Coast Air Quality Management District monitoring station, Anaheim, California. Samples were also taken from 23 March 1978 to 9 April 1978 and then continued from 19 February 1979 at Argonne, Illinois. All these samples were taken in parallel on 47-mm diameter Millipore filter membranes (1.2-μm nominal pore size, type RATF), which were used for the optical attenuation measurements, and prefired quartz fiber filters (Pallflex type 2500 QAO), which were used for the carbon determinations. The monitored flow rates varied between 1.0 and 2.6 m^3/cm^2-day (i.e., 0.24 to 0.62 CFM for the total exposed filter area of 9.6 cm^2), corresponding to face velocities of 11.6 to 30.1 cm/sec. The samples were not size segregated. A number of representative source particulates have also been sampled and analyzed. These include particles collected 1) in a freeway tunnel, 2) in an underground parking garage, 3) from a small 2-stroke engine, and 4) from a 4-stroke diesel engine. The optical attenuation is defined as

$$ATN = -100 \ln (I/I_0)$$

where I_0 is the intensity of the light (λ = .63 μ) transmitted through a blank Millipore filter and I is the intensity through a loaded filter. If we assume fixed optical constants, this quantity should be proportional to the "graphitic" content of the aerosol. The carbon loading on the quartz fiber filters was determined by a total combustion/CO_2 evaluation method.[8] The quartz filters were prefired overnight at 800°C to remove all combustible carbon before sample collection. Periodic analysis of blanks typically yielded about 0.5 μg C/cm^2, compared with loadings after exposure in the range 20-100 μg C/cm^2.

Photochemical gas-to-particle conversion reactions should be most pronounced in the summer in the Los Angeles air basin, while in the winter in Argonne or Berkeley, these reactions should play a much smaller role and the primary component should be much more important. These different photochemical conditions should manifest themselves in the ratio of the "graphitic" soot to total carbon content of the particles. That is, under highly photochemical conditions one would expect this ratio to be significantly smaller than under conditions obviously heavily influenced by sources. In view of the above, the graphs of optical attenuation versus carbon loading shown in Fig. 1 for samples collected at Berkeley, Fremont, and Anaheim, California, and Argonne, Illinois, as well as various combustion sources, are unexpected. Analyses of the data show that:

1. There is a strong correlation ($r > 0.85$) between optical attenuation and total suspended particulate carbon at every site.

2. The least squares fit of the data shows relatively small regional differences with a trend toward increasing slope (enrichment in primary carbonaceous matter) for samples collected respectively at Berkeley, Fremont, Anaheim, and Argonne.

3. There is a strong correlation between the optical attenuation and the carbon loading for the source samples, and the slope of the least squares fit is comparable to that found in the ambient samples.

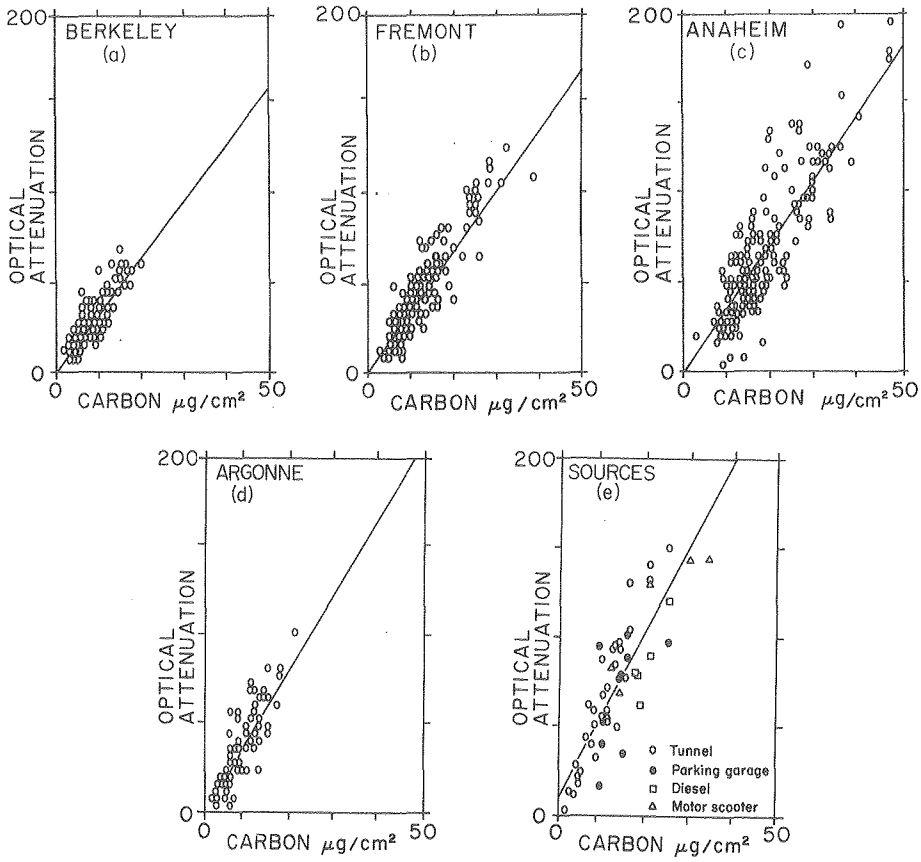

Fig. 1. Plots of optical attenuation versus carbon loading in $\mu g/cm^2$ for particulate samples collected at Berkeley, Fremont, Anaheim, and Argonne, and from various combustion sources. The solid line represents the least squares fit of the data points. (XBL 796-1920A)

Result 1 shows that it is possible to predict the total amount of particulate carbon with an RMS deviation of 30% by means of a simple measurement of optical attenuation. This implies that the fraction of "graphitic" soot to total particulate carbon is approximately constant under the wide range of conditions occurring at a given site. On specific days there can be large variations in the ratio, but no large systematic differences are found as a function of the ozone concentration, which has been viewed as a monitor of the photochemical activity. This is graphically demonstrated in Fig. 2, which shows the distribution of the ratios of the optical attenuation to total carbon content for ambient samples from all the California sites taken together, subdivided according to peak hour ozone concentration. Clearly there is no trend for high-ozone days to be characterized by aerosols which have a significantly reduced "graphitic" fraction. This places a rather low limit on the maximum importance of secondary organic particulates formed in correlation with the ozone concentration.

As seen in Fig. 1e, a strong correlation is also observed between the optical attenuation and the carbon content of the source samples. The slope of the least squares fit of the source data is somewhat larger than that found for the ambient samples, but there is still considerable overlap between the two data sets. This similarity in the absorbing properties of the ambient and source samples strongly suggests that a large component of the carbonaceous aerosol studied is of primary origin. However, due to the spread in both the ambient and the source data, these results do not exclude the possibility of significant secondary species produced in nonozone-related reactions. Indeed the results of Grosjean,[9] Gundel et al.,[10] and others[11] suggest that the polar component of the carbonaceous aerosol cannot be accounted for directly from primary emissions. The trend of the sources to have higher optical attenuation per unit carbon than that found in urban air may also be indicative of a secondary component. An analysis based on comparing the least squares fit of the source and ambient data at all sites is consistent with a secondary component, which ranges between 15 and 35% of the carbonaceous mass. The data presented here were taken in two California air basins and in the Chicago area. The generality of these results to other areas across the United States and in some areas of Europe is presently being tested. Preliminary data obtained on samples from New York City, Denver, Seattle, Portland, and Washington, D.C. are in agreement with the findings outlined in this paper.

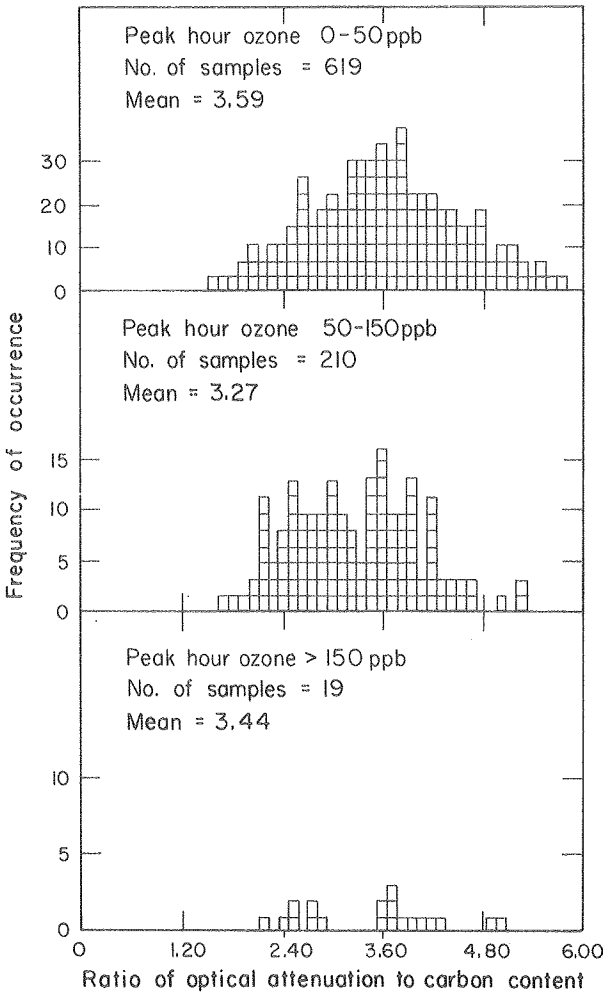

Fig. 2. Distribution of the ratios of optical attenuation to total carbon content in $\mu g/cm^2$ subdivided according to the peak ozone concentration. Note that the means of the distributions are only marginally smaller at larger ozone concentrations, which puts a rather low limit on secondary organics produced in correlation with ozone. (XBL 798-2704)

FOOTNOTE AND REFERENCES

*Published in Science 208, 741 (1980).

1. For a review of chemical mechanisms for secondary organic formation, see D. Grosjean, in Proceedings, Conference on Carbonaceous Particles in the Atmosphere, Lawrence Berkeley Laboratory Report LBL-9037, p. 107 (1979). (available from NTIS).

2. The use of the term "graphitic" is not meant to imply the three-dimensional structure of graphite, but only to indicate a structure similar to that of carbon black. This structure can be viewed to a first approximation as made up of small layered crystallites which have the hexagonal graphitic structure within aromatic planes but a random orientation of the planes about the C axis of the crystallites.

3. The hypothesis that much of the carbonaceous material in urban environments is soot was first advanced by T.Novakov, A. B. Harker, and W. Siekhaus, in Proceedings, First Annual NSF Trace Contaminants Conference (Oak Ridge National Laboratory Report CONF-730802, p. 354-379, 1974, available from NTIS). Additional results strengthening this hypothesis are in (a) T. Novakov, Proceedings, Second Joint Conference on Sensing of Environmental Pollutants (Pittsburgh, Instrument Society of America, 1973), pg. 197; (b) T. Novakov, S. G. Chang, and A. B. Harker, Science 186, 259 (1974); (c) S. G. Chang and T. Novakov, Atmos. Environ. 9, 495 (1975).

4. H. Rosen, A. D. A Hansen, L. Gundel, and T. Novakov, Applied Optics 17, 3859 (1978).

5. H. Rosen, A. D. A. Hansen, L. Gundel, and T. Novakov, in Proceedings, Conference on Carbonaceous Particles in the Atmosphere (Lawrence Berkeley Laboratory Report LBL-9037, p. 49, 1979, available from NTIS).

6. Z. Yasa, N. M. Amer, H. Rosen, A. D. A. Hansen, and T. Novakov, Applied Optics 18, 2528 (1979).

7. Preliminary evidence for the correlation between optical attenuation and total particulate carbon were presented by H. Rosen, A. D. A. Hansen, R. L. Dod, and T. Novakov, in Proceedings, Fourth Joint Conference on Sensing of Environmental Pollutants (Washington, American Chemical Society, p. 640, 1978); and by A. D. A. Hansen, H. Rosen, R. L. Dod, and T. Novakov in Proceedings, Conference on Carbonaceous Particles in the Atmosphere (Lawrence Berkeley Laboratory Report LBL-9037, p. 116, 1979, available from NTIS).

8. A similar system is described by P. K. Mueller, R. W. Mosley, and L. B. Pierce, in Proceedings, Second International Clean Air Congress (New York, Academic Press, 1971), p. 532.

9. D. Grosjean, Anal. Chem. 47, 797 (1975).

10. L. Gundel, G. E. Mason, and T. Novakov, in Atmospheric Aerosol Research Annual Report 1977-78 (Lawrence Berkeley Laboratory Report LBL-8686, p. 68, 1979).

11. See, for example, B. R. Appel, E. M. Hoffer, E. L. Kothny, S. M. Wall, M. Haik, and R. L. Knights, Environ. Sci. Technol. 13, 98 (1979).

APPLICATION OF THERMAL ANALYSIS TO THE CHARACTERIZATION OF NITROGENOUS AEROSOL SPECIES

R. Dod, et al.

In a previous report we described a combined optical attenuation-thermal analysis apparatus for the characterization of particulate carbonaceous aerosol material.[1] We have extended the use of this apparatus to include the simultaneous characterization of nitrogenous species.

A schematic representation of the apparatus used in our analysis of carbonaceous material is shown in Fig. 1. The particulate sample, collected on a prefired quartz filter, is placed in the quartz combustion tube so that its surface is perpendicular to the tube axis. The tube is supplied with purified oxygen, excess oxygen escaping through an axial opening at the end of the tube. The remainder of the oxygen (together with gases produced during analysis) passes through a nondispersive infrared analyzer (MSA LIRA 202S) at a constant rate. Sample carbon may be evolved through volatilization, pyrolysis, oxidation, or decomposition. To ensure complete conversion of this carbon to CO_2, a section of the quartz tube immediately outside the programmed furnace is filled with CuO catalyst, which is kept at a constant 900°C by a second furnace. This is especially necessary at relatively low temperatures when volatilization and incomplete combustion are the dominant processes occurring.

The actual measurement consists of monitoring the CO_2 concentration as a function of the sample temperature. The result is a "thermogram," i.e., a plot of the CO_2 concentration vs temperature, with the area under the thermogram proportional to the carbon content of the sample. The carbon content is quantitated by calibration with a calibration gas (CO_2 in oxygen) and by measuring the flow rate through the system. This calibration is cross-checked by analyzing samples of known carbon content.

The thermograms of ambient and source aerosol samples reveal distinct features in the form of peaks or groups of peaks. One important component of the carbonaceous aerosol is the "graphitic" carbon, which is known to cause the black or gray coloration of ambient and source particulate samples.[2] To determine which of the thermogram peaks corresponds to this "graphitic" carbon, we monitor the intensity of a He-Ne laser beam which passes through the filter. This provides simultaneous measurement of sample absorptivity and CO_2 evolution. The light penetrating the filter is collected by a quartz light guide and filtered by a narrow band interference filter to minimize the effect of the glow of the furnaces. An examination of the CO_2 and light intensity traces enables the assignment of the peak or peaks in the thermograms corresponding to the black carbon because they appear concurrently with the decrease in sample absorptivity.

The potential of this method (in the CO_2 mode) is illustrated in Fig. 2, where the complete thermogram of an ambient sample is shown. The lower trace represents the CO_2 concentration, while the

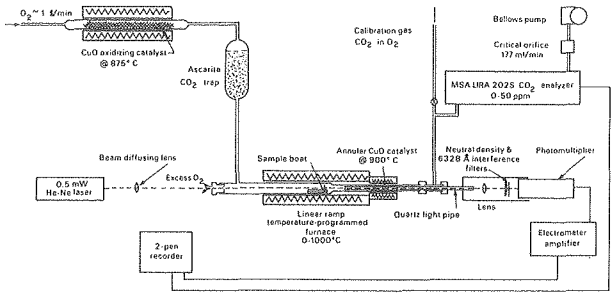

Fig. 1. Optico-thermal analysis apparatus. (XBL 791-167)

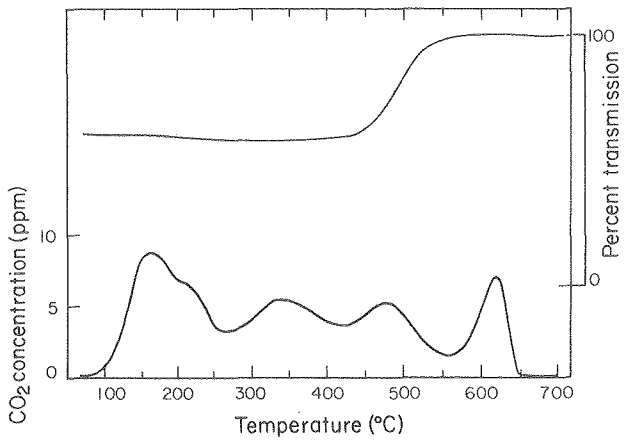

Fig. 2. CO_2 thermogram of Berkeley ambient aerosol particles (5/31/79). (XBL 807-1696)

upper curve corresponds to the light intensity of the laser light beam that reaches the detector during the temperature scan. Inspection of the thermogram shows that a sudden change in the light intensity occurs concomitantly with the evolution of the CO_2 peak at about 470°C. The light intensity I_0, after the 470°C peak has evolved, corresponds to that of a blank filter. This demonstrates that the light-absorbing species in the sample are combustible and carbonaceous, the "graphitic" carbon referred to above. The carbonate peak evolves at about 600°C; and as carbonate is not light absorbing, it does not change the optical attenuation of the sample. In addition to black carbon and carbonate, the thermogram in Fig. 2 also shows several distinct groups of peaks at temperatures below ~400°C that correspond to various organics.

We have expanded the capabilities of the thermal analysis method to nitrogenous species by connecting the outlet of the passive CO_2 analyzer through an orifice to a chemiluminescent NO_x analyzer (Thermo-Electron, Model 14D). No modifications were made to the combustion section of the

system or to the oxidation catalyst. The modified thermal analysis system was tested by analyzing known amounts of nitrogen-containing compounds. Examples of inorganic and organic standards are shown in Figs. 3-5.

Ammonium nitrate produces a sharp, single NO_x thermogram peak centered at about 160°C (Fig. 3). Ammonium sulfate results in a double peak located at about 210° and 270°C (Fig. 4). The fact that $(NH_4)_2SO_4$ produces a double peak suggests that this compound decomposes initially into ammonia and ammonium bisulfate (NH_4HSO_4). The NO_x peak for melamine is, as expected, coincident with the CO_2 peak at about 275°C (Fig. 5).

At present this method is in the developmental stage and therefore is not yet completely quantitative. We have nevertheless applied the method to analyze several ambient particulate samples. The principal reason for analyzing ambient samples was to see whether non-nitrate and non-ammonium nitrogenous species can be detected. Such species were identified in ambient particles by x-ray photoelectron spectroscopy (ESCA) but have not been clearly demonstrated by other techniques.

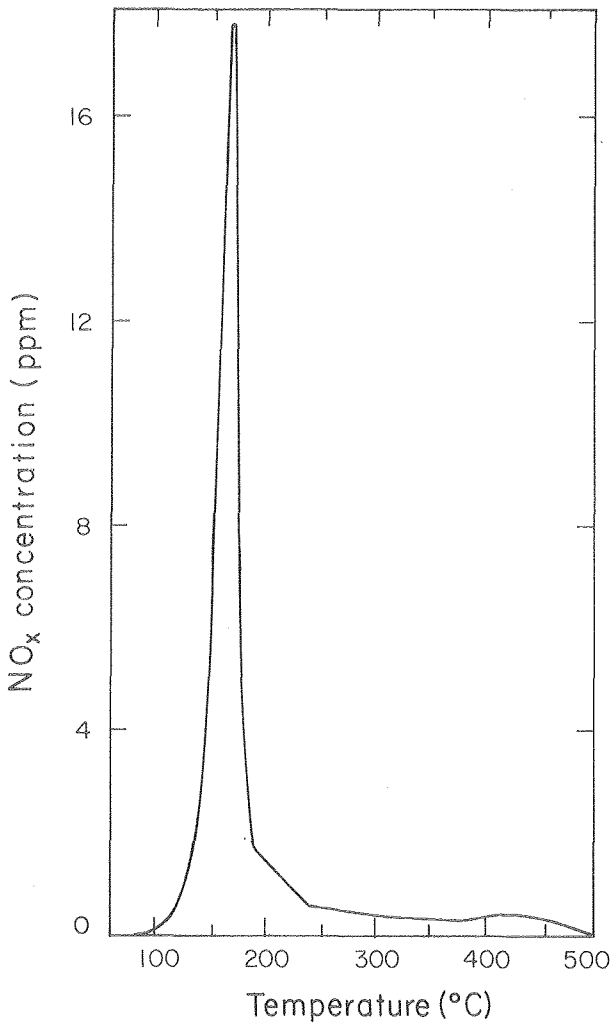

Fig. 3. NO_x thermogram of NH_4NO_3. (XBL 807-1693)

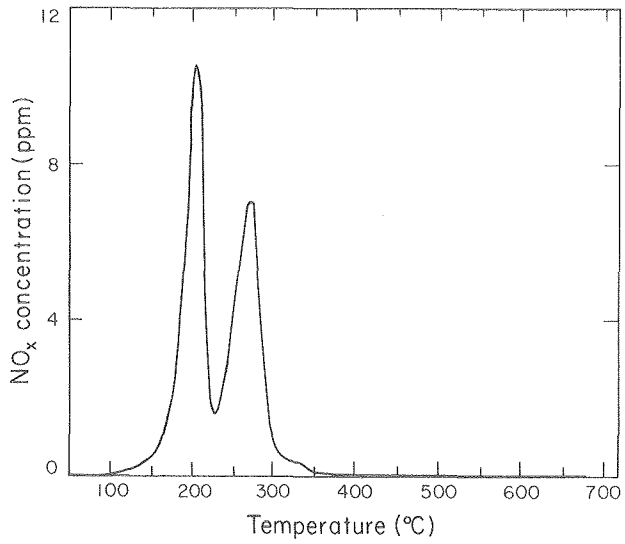

Fig. 4. NO_x thermogram of $(NH_4)_2SO_4$. (XBL 807-1694)

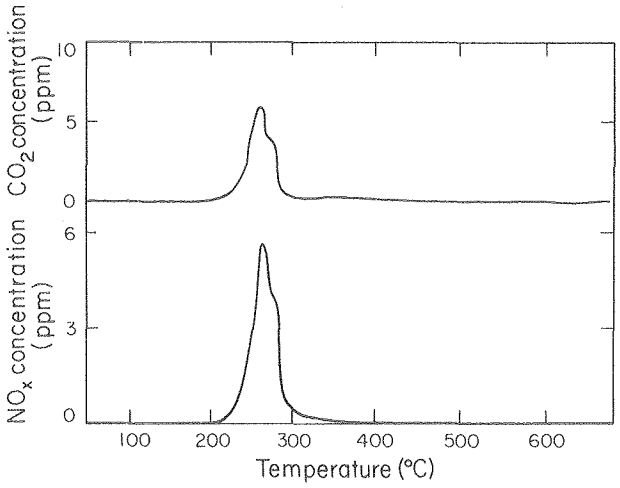

Fig. 5. NO_x thermogram of melamine. (XBL 807-1695)

Two examples of ambient sample NO_x, CO_2 thermograms are shown in Figs. 6 and 7. The thermogram of the sample collected on 4/26/79 at the NBS facility near Washington, D.C., shows that the principal nitrogen species is ammonium nitrate with a relatively small amount of ammonium sulfate. No other nitrogenous species were detected in this sample. The other sample (Fig. 7) shows that the ammonium sulfate and/or bisulfate are the principal nitrogen-containing species. Here, however, a broad peak in the NO_x thermogram is seen between 400° and 500°C, which can be attributed to a non-nitrate, non-ammonia, probably organic nitrogenous species. Similar broad peaks have been seen in thermograms of ambient species from other sites.

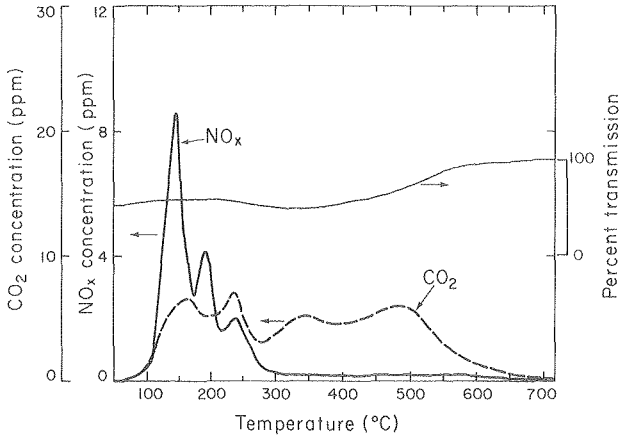

Fig. 6. CO_2/NO_x thermogram of Washington, D.C., ambient aerosol particles (4/26/79) (4.6 µg sulfur in sample). (XBL 807-1692)

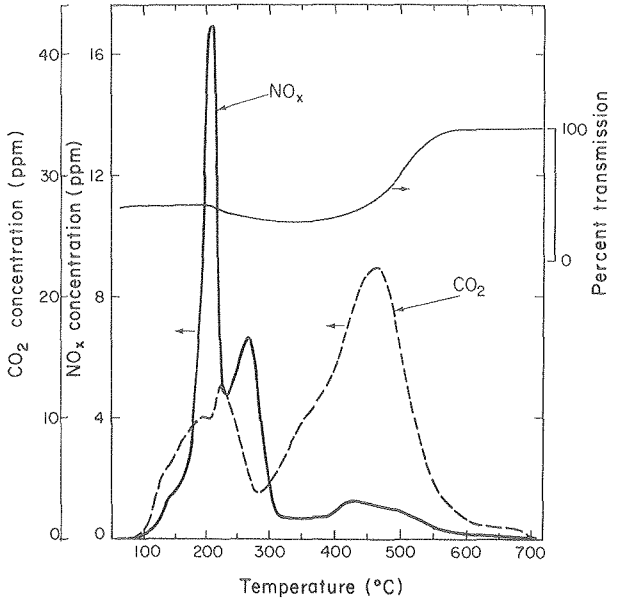

Fig. 7. CO_2/NO_x thermogram of Washington, D.C., ambient aerosol particles (4/24/79) (22.6 µg sulfur in sample). (XBL 806-1143)

REFERENCES

1. R. L. Dod, H. Rosen, and T. Novakov, "Optico-thermal analysis of the carbonaceous fraction of aerosol particles," Lawrence Berkeley Laboratory Report LBL-8698 (1978).

2. H. Rosen, A. D. A. Hansen, L. Gundel, and T. Novakov, "Identification of the optically absorbing component in urban aerosols," Appl. Opt. 17, 3859 (1978).

3. T. Novakov, P. K. Mueller, A. E. Alcocer, and J. W. Otvos, "Chemical composition of Pasadena aerosol by particle size and time of day. III. Chemical states of nitrogen and sulfur by photoelectron spectroscopy," J. Coll. Interface Sci. 39, 225 (1972).

APPLICATION OF SELECTIVE SOLVENT EXTRACTION AND THERMAL ANALYSIS TO AMBIENT AND SOURCE-ENRICHED AEROSOLS

L. Gundel, et al.

INTRODUCTION

Selective solvent extraction (SSE) has been used to characterize carbonaceous aerosol particles by estimating the fractions of "primary," "secondary," and "elemental" carbon in ambient and source aerosols.[1-5] This laboratory has recently developed a thermal analysis (TA) technique[6-7] which allows simultaneous measurement of light transmission through a filter and evolved CO_2 during its temperature-programmed combustion. In this study we use these techniques in a complementary manner by performing TA on particulate samples which have been subjected to SSE. The samples chosen for this study were collected during the same sampling periods at two locations in Berkeley, California--one close to a freeway and the other closer to our laboratory. The aims of this work include:

1. Comparison of average secondary:primary: elementary (S:P:E) ratios for these two sites to each other and to ratios obtained previously[5] for source and ambient particulate manner.

2. Comparison of thermal analysis results for the two sites.

3. Observation of the effects of SSE on thermogram "fingerprint" features to enable solubility characterization of the typical "volatile," "high molecular weight," and "high temperature" peaks.

4. Characterization of "primary" and "secondary" carbon by construction of difference thermograms.

5. Comparison of "elemental" carbon as defined by SSE to optically absorbing or "black" carbon.

EXPERIMENTAL DETAILS

High volume samplers were operated simultaneously for 24-hour periods at 40 SCFM at a freeway sampling site located about 200 feet east of the Bayshore Freeway and at LBL, about 700 feet above sea level, 4 miles east of the freeway sampling site. Usually the prevailing winds were from the west toward the LBL site. The filter samples were collected on prefired quartz during September, 1979. During the sampling period, 17-20 September 1979, there were night and morning low clouds which cleared by midmorning. Maximum and minimum temperatures averaged 73° and 62°F respectively. Average ozone level was 20 ppb during this week.

Selective solvent extraction was performed on the three pairs of samples. The soxhlet extraction technique has been described previously.[3-5] Cyclohexane was used to extract a piece of filter 50 cm^2 in area; another section of filter of the same area was sequentially extracted in benzene and in a methanol-chloroform (1:2 v:v) mixture. All solvents were spectral grade and residue free. Fractions of "primary," "secondary," and "elemental" carbon were determined according to a procedure described by Appel et al.[3,5]: "primary" carbon is cyclohexane-extracted carbon; "secondary" carbon is the difference between the total carbon extracted by the benzene, methanol-chloroform sequence and the cyclohexane-extracted carbon. "Elemental" carbon is the difference between total carbon and carbon extracted by the benzene, methanol-chloroform sequence. "Primary," "secondary," and "elemental" carbon fractions of the total carbon were determined using both the evaporated extracts and the extracted filters so that two sets of numbers were computed for each filter. Thermal analysis was performed on 1.69 cm^2 sections of the extracted and unextracted filters.

RESULTS

Figure 1 contains the SSE results for the three pairs of filter samples, along with results obtained earlier[5] for particulate matter collected at the LBL site and in the Caldecott Tunnel. Figure 1a represents the results based on combustion of evaporated extracts; Fig. 1b displays the results based on combustion of the extracted filters. Losses of volatile carbon during extraction[5] and esterification of some organic components[5] may make the "primary" carbon percentage low and the "secondary" component high when evaporated extract results are compared to results based on combustion of the extracted filters.

Comparison of the newer SSE results for the LBL sampling site with results obtained in the summer of 1978 shows that the same patterns exist in S:P:E ratios, but the recently collected particulate samples contain somewhat less "elemental" and more "secondary" than the earlier samples do, based on combustion of extracted filters. Particulates collected near the freeway contain less "secondary," more "primary" and more "elemental" carbon than do particulates collected at the LBL site. S:P:E ratios are 22:23:55 compared to 40:26:34, respectively, based on combustion of extracted filters. Ratios based on evaporated

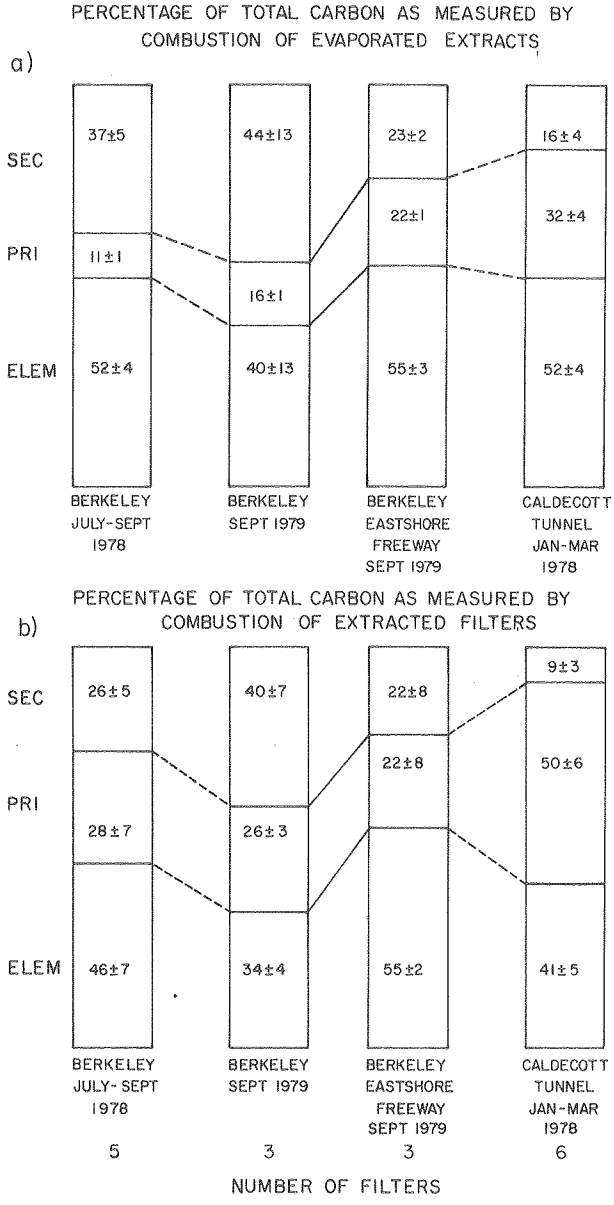

Fig. 1. Selective solvent extraction results expressed as a percentage of total original carbon. "ELEM" = "elementary" carbon = carbon insoluble after successive extraction with benzene followed by a methanol-chloroform mixture; "PRI" = "primary" = cyclohexane-soluble carbon; "SEC" = "secondary" = difference between total soluble carbon and cyclohexane-soluble carbon. (XBL 801-109)

extracts show the same trend. The average total carbon at the freeway is 2.1 times that at LBL. Particulates collected near the freeway contain more "secondary," less "primary," and more "elemental" carbon than do particulates collected in the Caldecott Tunnel during 1978, based on combustion of extracted filters: S:P:E ratios are 22:23:55 and 9:50:41 respectively.

Thermograms of one pair of particulate loaded filters are presented in Fig. 2. Figure 2a shows

thermograms for the LBL sampling site. Figure 2b contains difference thermograms for the same filter. The "primary" carbon difference thermogram was obtained by subtraction of the cyclohexane-extracted filter thermogram from the thermogram for the unextracted filter. The "secondary" carbon difference thermogram was obtained by subtracting the benzene, methanol-chloroform-extracted filter thermogram from the cyclohexane-extracted filter thermogram. The "elemental" carbon thermogram is the benzene, methanol-chloroform-extracted filter thermogram. The temperature midpoint in optical transmission change is indicated on each part of the figure. The same information is provided for the corresponding freeway particulate sample in parts c and d of Fig. 2. Thermograms for the other two pairs of filters show the same effects as those discussed below. The following observations can be made from study of these thermograms:

1. For particulate samples from both sites, cyclohexane extraction removes most of the low temperature or "volatile" carbon, part of the "higher molecular weight" carbon, and little of the "black" carbon, since the optical transmission is not affected by cyclohexane extraction. The "primary" carbon difference thermograms contain most of the structural features of the original thermograms. The CO_2 maxima in the "primary" carbon thermograms correspond to the "volatile" carbon peak of the unextracted filters.

2. For particulate samples from both sites, sequential benzene and methanol-chloroform extraction removes the low temperature or "volatile" carbon, as well as part of the "high molecular weight" carbon. The optical transmission is not affected by sequential benzene and methanol-chloroform extraction. The "secondary" carbon difference thermograms show maxima between 300 and 450°C.

3. Nonextractable or "elemental" carbon from both sites contains organic material which does not absorb light, with combustion temperature peaks at about 325°C, in addition to "black" or "graphitic" carbon with combustion peaks at about 480°C. This means that nonextractable carbon cannot be equated with elemental or "graphitic" carbon.

4. Since the high-temperature peak from both sites contains some extractable carbon in addition to "black" carbon, "high temperature" carbon cannot be equated with "black" carbon.

5. The complementary use of SSE and TA makes it possible to determine the fraction of "black" carbon in these particulate samples. For the LBL site and the freeway site, the fractions of "black" carbon are 0.235 and 0.383 respectively.

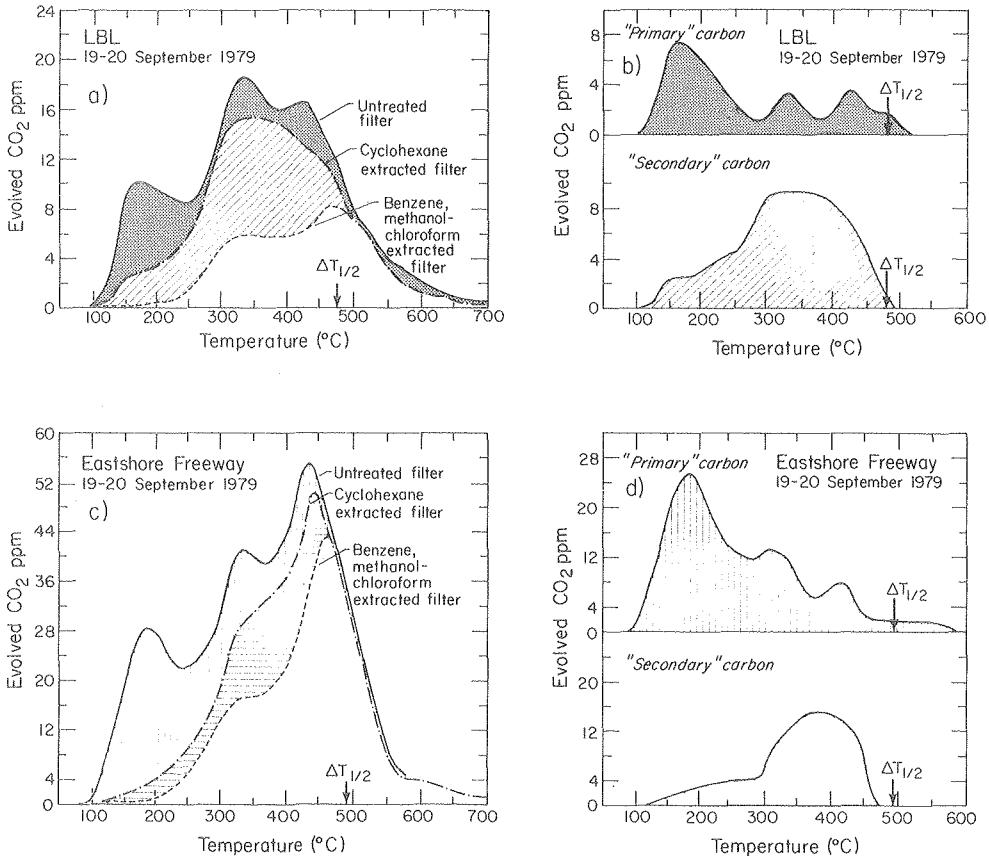

Fig. 2. Thermal analysis results for particulate matter collected at LBL and at a site near the Eastshore Freeway. The temperature midpoint in the optical transmission change is indicated as $\Delta T_{1/2}$. (XBL 801-110)

DISCUSSION AND CONCLUSION

Thermal analysis of extracted filters provides further characterization of carbonaceous particulates than can be achieved with either TA or SSE alone. It is now possible to determine the amounts of "black" carbon in particulate matter using combined selective solvent extraction and thermal analysis. We plan to extend these preliminary measurements to study particulates collected by low-volume samplers in several urban areas throughout the United States.

REFERENCES

1. D. Grosjean, "Solvent extraction and organic carbon determination in atmospheric particulate matter: The organic extraction-organic carbon analyzer (OE-OCA) technique," Anal. Chem. 47, 797 (1975).

2. B. R. Appel, P. Colodny, and J. J. Wesolowski, "Analysis of carbonaceous materials in southern California atmospheric aerosols," Environ. Sci. Technol. 10. 359 (1976).

3. B. R. Appel, E. M. Hoffer, M. Haik, S. M. Wall, E. L. Kothny, R. L. Knights, and J. J. Wesolowski, Characterization of Organic Particulate Matter, Final Report to California Air Resources Board, Contract No. ARB 5-682 (1977).

4. B. R. Appel, E. M. Hoffer, E. L. Kothny, S. M. Wall, M. Haik, and R. L. Knights, "Analysis of carbonaceous material in southern California atmospheric aerosols," Environ. Sci. Technol. 13, 98 (1979).

5. L. A. Gundel, G. E. Mason, and T. Novakov, "Characterization of source and ambient particulate samples by solvent extraction," in Atmospheric Aerosol Research Annual Report 1977-78, LBL-8696 (1979), p. 63.

6. R. L. Dod, H. Rosen, and T. Novakov, "Optico-thermal analysis of the carbonaceous fraction of aerosol particles," in Atmospheric Aerosol Research Annual Report 1977-78, LBL-8696 (1979), p. 2.

7. R. S. Dod, this report, previous article.

DETERMINATION OF CARBON IN ATMOSPHERIC AEROSOLS BY DEUTERON-INDUCED NUCLEAR REACTIONS

M. Clemenson, et al.

INTRODUCTION

Carbon has been found to be a major constituent of urban particulate pollution.[1,2] The determination of the origin of the carbon in terms of primary and secondary components is a difficult problem to which a solution is necessary if meaningful control strategies are to be implemented. Some work has been done, but much more work is required.[3,5] Of important analytical concern is the nondestructive determination of the total carbon content of atmospheric aerosol samples. The common method of carbon determination in atmospheric aerosol samples is by combustion analysis. This method, however, is destructive of the sample and thus does not allow other analyses to be performed on the same sample. A new method for the nondestructive determination of carbon and other low-Z elements in atmospheric aerosols has been developed by Macias and coworkers.[6] Their method involves the in-beam measurement of γ rays from the inelastic scattering of 7-MeV protons accelerated in a cyclotron. This type of analysis requires lengthy use of accelerator time. Another method for the nondestructive determination of carbon has been developed by Gordon and coworkers.[7] This involves the measurement of prompt γ rays following neutron capture; they use an external beam port of the National Bureau of Standards (NBS) research reactor as the neutron source. Relatively large samples ($\sim$1 g), however, and long irradiation periods ($\sim$20 hr) are required. A new activation-analysis method for the determination of carbon in atmospheric aerosols using only a short amount of beam time (2 min) will be described here. This method has already been used to determine nitrogen in aerosols and future work will center on the development of a method for the determination of oxygen in aerosols.[8]

Other nondestructive methods can be used for the determination of elemental concentrations in atmospheric aerosols. The most commonly used methods are x-ray fluorescence analysis and neutron activation analysis; neither is suitable for the determination of low-Z elements. The x-ray fluorescence method is of great importance for the sensitive and nondestructive determination of elements as light as sulfur, but for elements lighter than sulfur two effects limit its usefulness: (a) the fluorescence yield drops to the range of a few percent for these elements and (b) there are large x-ray absorptive effects because of the very low energy of the x rays (<0.5 keV). Neutron activation analysis for low-Z elements is limited by unfavorable nuclear properties of the important nuclides in this area. The thermal-neutron absorption cross sections are very small for the important reactions. The induced radioactivities are also unsuitable for counting because of very long or very short half lives.

The deuteron activation analysis takes advantage of favorable nuclear properties and

cross sections. Carbon is detected by the use of deuterons to induce the $^{12}C(d,n)^{13}N$ reaction. The decay of the 10.0-min ^{13}N is followed by its 0.511-MeV annihilation radiation using γ-ray spectrometry. The use of activation analysis for elemental determinations has reached into almost every field where sensitive and nondestructive analyses are required. The general principles of charged-particle activation analysis have been discussed by Markowitz and Mahony.[9] New advances in the field of activation analysis have been reviewed in a recent article by Lyon and Ross.[10]

EXPERIMENTAL

Targets

The targets used to determine the $^{12}C(d,n)^{13}N$ excitation function were 2 mg/cm^2 polystyrene foils, $(C_8H_8)_n$. The targets were 2.2-cm diameter and the deuteron beam was collimated into a 1.3-cm diameter central spot. Polystyrene was selected for its purity and high carbon content of 92.3% C.

Irradiations

The Lawrence Berkeley Laboratory 88-inch cyclotron facility was used for the irradiations. Aluminum foils were used to degrade the beam from the initial energy to the desired energy. The range-energy tables of Williamson, Boujot, and Picard were used to calculate the required aluminum thickness.[11] The targets were irradiated at different energies by the stacked-foil technique. The targets were typically irradiated for 2 minutes at an average beam intensity of 0.5 μA. The total charge received by the Faraday cup was measured by an integrating electrometer.

Counting

The irradiated samples were analyzed by detecting the 0.511-MeV positron-annihilation radiation of ^{13}N. The counting system consisted of a high-resolution Ge(Li) detector and fast electronics coupled to a 4096-channel computer-controlled analyzer. The data were recorded on magnetic tape for later analysis. The Ge(Li) detector used for this work has an active volume of 60 cm^3. The resolution of the detector is 2.0 keV (full-width at half-maximum) at the 1.3325 MeV γ-ray of ^{60}Co. The use of this system allowed the collection of γ-ray information up to 2.0 MeV with excellent resolution. The information obtained permitted a more complete identification of other radionuclides produced during the irradiation and also protected against γ-ray interferences that might not be detected with a low-resolution system such as a NaI spectrometer (6-7% resolution). In routine use a simple counting system consisting of a NaI detector and a single-channel analyzer could be used after the high-resolution system has demonstrated that there are no γ-ray interferences with the 0.511-MeV annihilation radiation.

The decay of the 0.511-MeV annihilation-radiation activity of an activated (E_d = 8.6 MeV) polystyrene target is shown in Fig. 1. The decay is a single component with a half life of 10.0 min corresponding to the decay of ^{13}N in the target.

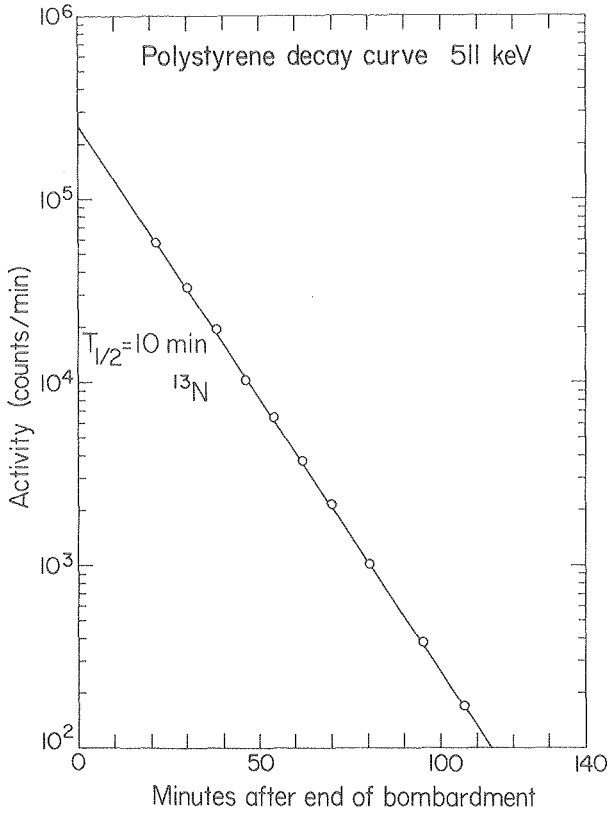

Fig. 1. Decay of the 0.511-MeV annihilation radiation activity following deuteron irradiation of a polystyrene foil. (XBL 797-2330)

The samples were counted approximately 5 cm from the face of the Ge(Li) crystal. In this geometry, the 0.511-MeV γ-ray overall detection coefficient (ODC) was 0.97%. ODC ≡ (c/m) in the photopeak/(d/m) from the standard source. It was determined with a ^{22}Na calibrated standard, obtained from the International Atomic Energy Authority, Vienna. The decay curves were analyzed with the CLSQ computer code.[12]

RESULTS

Excitation Function

The absolute cross sections at several energies were determined for the $^{12}C(d,n)^{13}N$ reaction with the polystyrene foils (Fig. 2). The excitation function measured in 1959 by Brill and Sumin[13] agrees well with our result. The estimated accuracy of the excitation function is approximately 5%. The production of ^{13}N from ^{13}C (1.11% abundance) was neglected. The uncertainties in the measurement include: (a) statistical fluctuations in the counting rates, (b) decay-curve component resolution, (c) determination of the integrated charge, (d) measurement of the weight of the polystyrene foils, and (e) the determination of the overall detection coefficient.

Inteferences

Two types of interferences that must be considered in charged-particle activation analysis

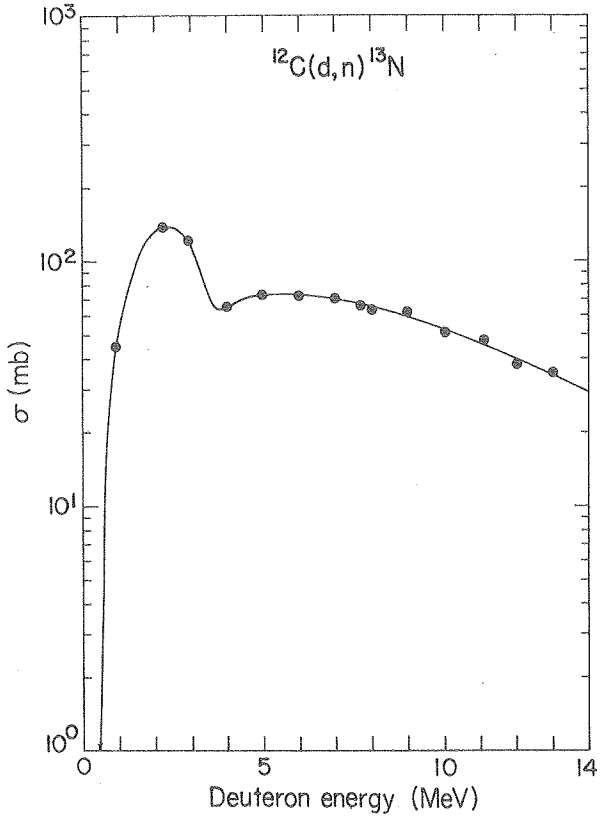

Fig. 2. Excitation function for the $^{12}C(d,n)^{13}N$ reaction. (XBL 797-2331)

using γ-ray spectroscopy to detect the 0.511-MeV annihilation radiation are: (a) the production of positron-emitting activities of similar half life to the activity of interest, and (b) the production of the activity of interest from elements other than the one under analysis. Because the annihilation radiation is only characteristic of a positron decay event, all positron-emitting nuclides will contribute to the 0.511-MeV radiation. The activities must be separated by their half lives in a decay curve analysis. The possible interfering radionuclides must be identified and their importance carefully investigated. The production of positron-emitting activities of similar half life to ^{13}N ($t_{1/2}$ = 10.0 min) is not a serious problem with the carbon determination because the ^{13}N activity is by far the dominant positron-emitting activity, and it is easily resolved in the decay-curve analysis.

Interfering reactions can sometimes be avoided by selection of the incident particle energy to be below the reaction threshold. The possible interfering reactions of importance are listed in Table 1. The reaction used for the determination of carbon is listed first. If the sample is irradiated with deuterons of energy less than 8 MeV, the $^{14}N(d,dn)^{13}N$ and $^{16}O(d,\alpha n)^{13}N$ interfering reactions will be energetically forbidden. The $^{14}N(d,t)^{13}N$ reaction cross section was measured (with GaN as target) at a deuteron energy of 7.6 MeV and found to be 1.3 mb. This cross section is much smaller than the $^{12}C(d,n)^{13}N$ cross section at this energy (σ= 70 mb). Furthermore, typical atmospheric aerosols contain 4 to 8 times as much carbon as nitrogen. Nitrogen, therefore, does not constitute an interference. The aerosol samples were irradiated at a deuteron energy of 7.6 MeV.

Table 1. Nuclear reaction thresholds for the reaction of interest and the principal interfering reactions.

Reaction	Threshold, MeV
$^{12}C(d,n)^{13}N$	0.33
$^{14}N(d,t)^{13}N$	4.91
$^{14}N(d,dn)^{13}N$	12.06
$^{16}O(d,\alpha n)^{13}N$	8.37

Aerosol Sample Analyses

The atmospheric aerosol was collected on a silver-membrane filter with the use of a vacuum pump. Silver filters are the best commercially available filter for the analysis of aerosol samples using deuteron activation analysis. Because silver has a high atomic number, the Coulomb barrier can be used to minimize deuteron reactions on the filter material. The relatively massive filter (40 mg Ag/cm^2) is only slightly activated. This permits the most sensitive detection of the γ radiation from the activation of the aerosol itself. The deuteron energy of 7.6 MeV that was used for the irradiation of the filter sample is below the Coulomb barrier of 8.4 MeV for deuterons plus silver.

The typical loading of particulates on the silver filter was approximately 250 μg/cm^2. A stacked-foil arrangement was used for the irradiations. In the stack was a polystyrene foil used as the carbon standard, a filter sample, and aluminum foils. The aluminum foils were used to degrade the beam energy to the desired value. The polystyrene standard was irradiated at a deuteron energy of 8.6 MeV. The filter sample was irradiated at a deuteron energy of 7.6 MeV. The stack was typically irradiated for 2 minutes at a beam intensity of 0.5 μA.

The decay of the 0.511-MeV annihilation radiation was followed for 2 to 3 hours. A typical gamma-ray spectrum of an aerosol sample is shown in two parts in Figs. 3 and 4. Figure 3 shows the region between 0 and 1 MeV. Besides the annihilation radiation, several γ rays are present. Most of these γ rays are a result of the activation of the silver filter. The γ-ray at 844 keV, however, is due to the production of ^{27}Mg by the $^{27}Al(d,2p)^{27}Al$ reaction. The ^{27}Mg activity is a result of deuteron reactions involving the aluminum in the particulate matter and in the aluminum foil used to degrade the beam energy. The reaction products from the aluminum foil recoil into the filter sample and are stopped. Figure 4 shows the region

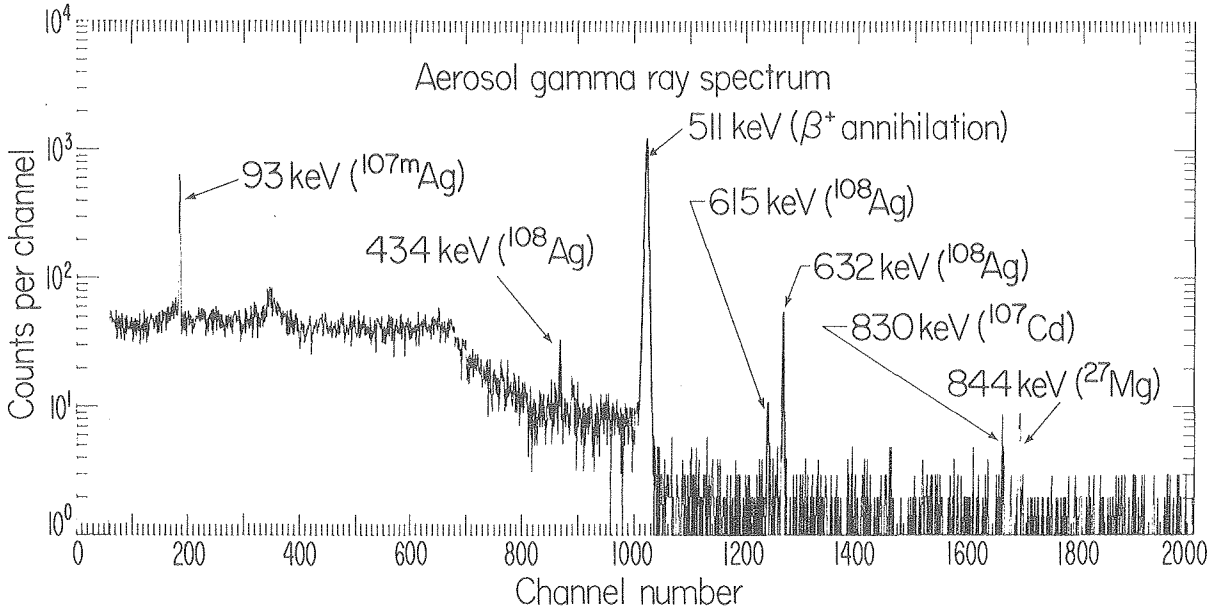

Fig. 3. The region from 0 to 1 MeV in the gamma ray spectrum of an aerosol sample following deuteron irradiation. (XBL 797-2335)

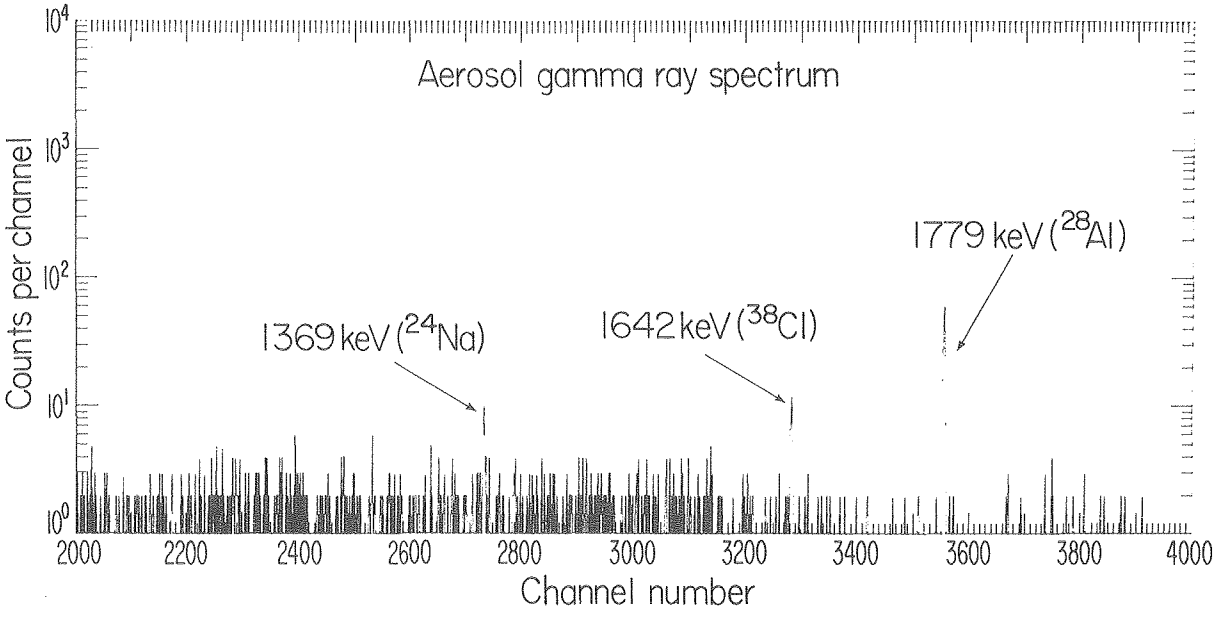

Fig. 4. The region from 1 to 2 MeV in the gamma ray spectrum of an aerosol sample following deuteron activation. (XBL 797-2336)

of the γ-ray spectrum between 1 and 2 MeV. Three γ-rays are observed in this region. The γ-ray at 1779 keV is from deuteron reactions involving aluminum. The ^{28}Al activity is produced by the ^{27}Al(d,p)^{28}Al reaction. The γ-ray at 1642 keV is from the production of ^{38}Cl in the aerosol by the ^{37}Cl(d,p)^{38}Cl reaction. The γ-ray at 1369 keV is due to ^{24}Na produced by deuteron reactions involving aluminum.

A typical decay curve for the integrated 0.511-MeV peak of an aerosol sample following deuteron irradiation is shown in Fig. 5. The end-of-bombardment counting rate, A_0, for the ^{13}N component in the aerosol was compared to the A_0 value for the ^{13}N component in the carbon standard. The carbon content of the aerosol was calculated relative to the carbon content of the standard. A carbon blank of approximately 0.5 μg/cm^2 was

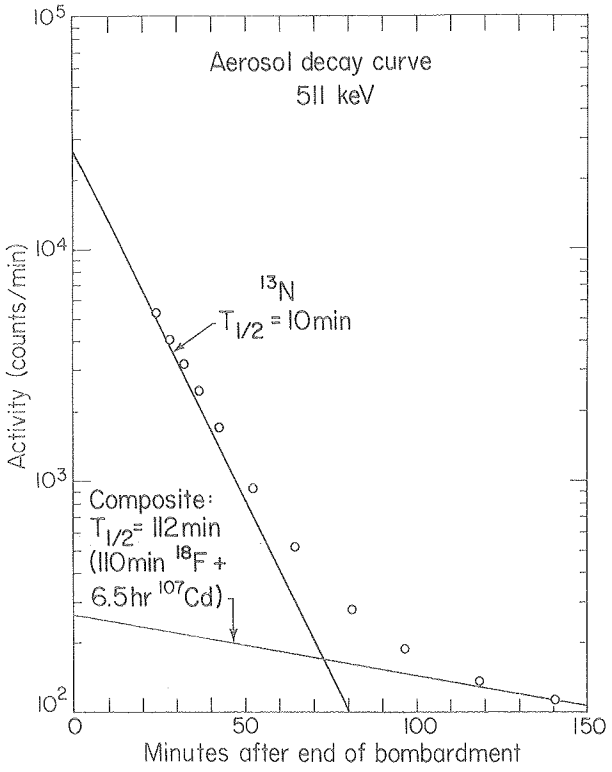

Fig. 5. Decay of the 0.511-MeV annihilation radiation activity following deuteron irradiation of an atmospheric aerosol sample. (XBL 797-2332)

found after the filters had been heated to 300°C for 24 hours; unheated Ag has a C content of approximately 5 μg/cm^2.

The deuteron activation method was used to analyze nondestructively samples containing varying amounts of carbon. The samples were subsequently analyzed for carbon in two separate laboratories using destructive combustion methods. The results of these analyses are summarized in Table 2. The samples can be divided into two groups. One group was prepared in the laboratory by depositing pure ammonium oxalate, $(NH_4)_2C_2O_4$, on a silver-membrane filter. These samples correspond to the first five listed in Table 2. The second group of ten samples are ambient aerosols collected in the San Francisco Bay Area.

Comparison of the carbon found by deuteron activation analysis and that found by the independent combustion methods shows a standard deviation of 10% for the 15 samples that were analyzed, i.e., $\bar{R}$, the ratio of C found by activation to C found by combustion, = 1.01 ± 0.10. The agreement holds over a wide range of carbon contents from 0.6 to 268 μg C/cm^2. The agreement is good for both the laboratory-prepared samples and the ambient aerosol samples.

The detection limit is estimated from a reasonable set of irradiation and counting conditions. The irradiation is carried out for three minutes at a deuteron beam intensity of 0.5 μA. The filter sample is irradiated at a deuteron energy of 7.6 MeV at which the $^{12}C(d,n)^{13}N$ reaction cross section is 70 mb. The overall detection coefficient for the annihilation radiation of ^{13}N is approximately 2%. The minimum activity that can be detected easily with reasonable precision is approximately 1000 counts/minute of ^{13}N at the end of bombardment. The minimum A_0 value takes into account the contribution of the other positron-emitting nuclides that are always present. Under these conditions the carbon detection limit is approximately 0.5 μg/cm^2; for an aerosol loading of 250 μg/cm^2, this corresponds to a C concentration of 0.2%.

REFERENCES

1. Proceedings of the Conference on Carbonaceous Particles in the Atmosphere, T. Novakov, Ed., Lawrence Berkeley Laboratory Report LBL-9037 (1979).

2. "Atmospheric Aerosol Research Annual Report, 1977-78," H. Rosen, ed., Lawrence Berkeley Laboratory Report LBL-8696 (1978).

3. H. Rosen, A. D. A. Hansen, R. L. Dod, and T. Novakov, "Soot in urban atmospheres: determination by an optical absorption technique," Science 208, 741 (1980).

4. D. Grosjean, in Proceedings of the Conference on Carbonaceous Particles in the Atmosphere, T. Novakov, ed., Lawrence Berkeley Laboratory Report, LBL-9037, 107 (1979).

5. R. L. Dod, H. Rosen, and T. Novakov, Lawrence Berkeley Laboratory Report LBL-8696, 2 (1978).

6. E. S. Macias, C. D. Radcliffe, C. W. Lewis, and C. R. Sawicki, Anal. Chem. 50, 1120 (1978).

7. M. P. Failey, D. L. Anderson, W. H. Zoller, G. E. Gordon, and R. M. Lindstrom, Anal. Chem. 51, 2209 (1979).

8. M. Clemenson, T. Novakov, and S. S. Markowitz, Anal. Chem. 51, 572 (1979).

9. S. S. Markowitz and J. D. Mahony, Anal. Chem. 50, 80R (1978).

10. W. S. Lyon and H. H. Ross, Anal. Chem. 50, 80R (1978).

11. C. F. Williamson, J. P. Boujot and J. Picard, Centre d'Etudes Nucleaires de Saclay, France, Report CEA-R 3042 (1966).

12. J. B. Cumming, in "Applications of Computers to Nuclear and Radiochemistry," G. D. Kelley, Ed., National Academy of Science-National Research Council, Nucl. Sci. Ser., NAS-NS 3107, 25 (1963).

13. O. D. Brill and L. V. Sumin, Atomnaya Énergiya 7, 377 (1959).

Table 2. Comparison of methods for carbon determination in atmospheric aerosols.

Sample	Material	C found, $\mu g/cm^2$ Deuteron activation	Combustion	Ratio (actv./comb.)
AO-1	ammonium oxalate	218	210	1.04
AO-2	ammonium oxalate	268	224	1.20
AO-3	ammonium oxalate	131	122	1.07
AO-4	ammonium oxalate	74	62	1.19
AO-5	ammonium oxalate	109	113	0.96
AA-1	aerosol	84	85	0.99
AA-2	aerosol	100	99	1.01
AA-3	aerosol	106	111	0.95
AA-4	aerosol	76	76	1.00
AA-5	aerosol	103	100	1.03
AA-6	aerosol	93	93	1.00
AA-7	aerosol	5.2	4.8	1.08
AA-8	aerosol	0.6	0.7	0.86
AA-9	aerosol	57	62	0.92
AA-10	aerosol	28	32	0.88
				$\bar{R} = 1.01 \pm 0.10$

INVESTIGATION OF SAMPLING ARTIFACTS IN FILTRATION COLLECTION OF CARBONACEOUS AEROSOL PARTICLES

R. Dod, et al.

INTRODUCTION

Carbon is a major fraction of the ambient atmospheric aerosol and is usually sampled by collecting particles on a filter. Questions have been raised as to how well the particles collected on a filter represent those actually present in the air.[1-4] Speculations regarding sampling artifacts have included adsorption and desorption of carbonaceous compounds from the collected particles and filter material as well as chemical transformations which would affect the volatility of some compounds. We have applied optico-thermal combustion analysis as well as total carbon combustion analysis to samples collected on pre-fired quartz fiber filters in an effort to elucidate the magnitude of some of these effects.

EXPERIMENTAL METHODS

The experimental configuration initially used was a filter stack of two quartz fiber filters inserted into a single 47-mm low-volume filter holder. Because of questions regarding the potential physical transfer of liquid aerosol from the first to the second filter, a series filter configuration was adopted consisting of an open-face 47-mm filter holder followed by an in-line 47-mm filter holder with a separation between the two of 5 cm. The filter medium in all cases was Pallflex 2500 QAO quartz fiber filters, which had been fired at 800°C for 2-6 hours to remove all combustible carbon. The face velocity for sampling was chosen to be approximately 0.18 m/sec to correspond to that typically used in our continuing ambient aerosol

sampling program. Tests were made at face velocities up to 0.40 m/sec, which approximates the face velocity in an 8" x 10" hi-volume sampler operating at 40 cfm. In order that sufficient sample could be collected for the analytical procedures used, the minimum sampling time was approximately 24 hours, with maximum sampling time of 7 days. Total carbon combustion analysis was done using a technique derived from that of Mueller[5] and the optico-thermal combustion analysis was done as described elsewhere.[6]

As a further check on the compatibility of this low-volume sampling technique with the standard hi-volume sampler, parallel samples at comparable face velocities showed no difference, either in total carbon or in type of carbon as determined by optico-thermal analysis.

As shown in Fig. 1. the carbon particulate loading in the air at our Berkeley sampling site has not changed greatly over a four-month period through the fall of 1979. However, the amount of carbon present on the second (in-line) filter has changed by about a factor of two over the same period from approximately 15% of the open-face loading to only about 8%. This relative change may be indicative of some type of annual variation in vapor phase or volatile carbon composition. The mean fraction of carbon found on the second filter shows no variation with sampling time (Table 1), indicating that if a saturation effect is operative, it was not reached in the sampling times investigated.

While the open-faced filter had in all cases a grey or black deposit, the second filter was in each case unsoiled, indicating that very few if any of the solid particles penetrated the first filter. The carbon present on the second filter must therefore be adsorbed hydrocarbon, either adsorbed from the ambient air or from material desorbed or vaporized from the first filter. Optico-thermal analysis shows that the material present on the second filter is primarily detected below ~250°C (Fig. 2), which from previous experiments indicates that it is due to small volatilizable organic compounds. Based on these results and from the apparent lack of saturation, it would seem reasonable to attribute the carbon on the second filter to vapor phase compounds adsorbed from the ambient air onto the quartz filter medium, with the adsorption being of sufficient strength not to be reversed under most ambient conditions. As a check of this, portions of one of the second filters were analyzed and the remainder of the filter was placed in a drying oven in air for 24 hours at 40-45°C; approximately 55% of the carbon was lost in this heating process.

The information gained to date is as conflicting as that which is already in the literature. Effects which have been observed could be due either

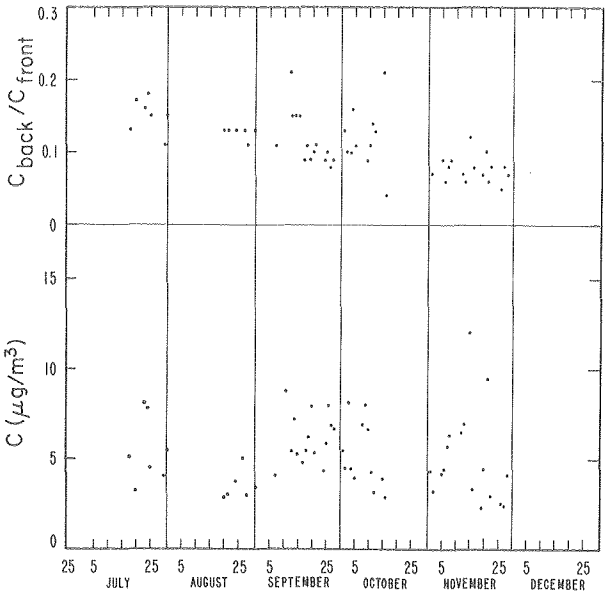

Fig. 1. a) Carbon on second filter as a fraction of carbon on open face filter.
b) Ambient carbon loadings from total carbon analysis of open face filter.
(XBL 806-1144)

Table 1. Carbon determined on second filters as a fraction of open-face filters.

Sampling time (days)	Number of samples	Carbon on second filter / Carbon on open-face filter
1	26	0.12 ± 0.04
2	2	0.14 ± 0.01
3	7	0.13 ± 0.02
4	1	0.11
5	1	0.15
7	1	0.13

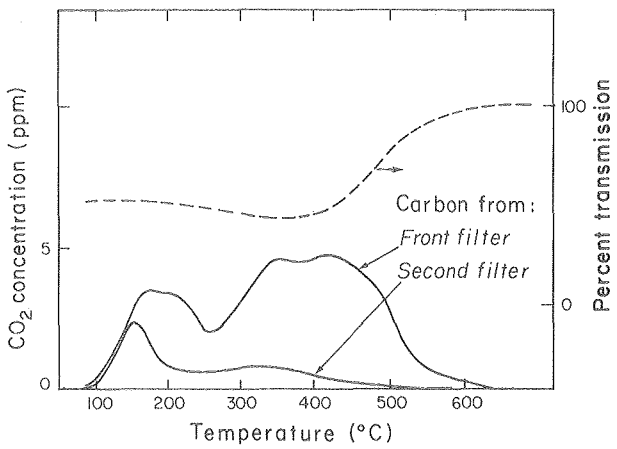

Fig. 2. Optico-thermal ayalysis of a typical Berkeley ambient series filter pair. (XBL 806-1146)

to gain or loss of "particulate carbon" on the filter. It is planned to continue this examination for a longer period of time to discover whether or not an annual cycle exists as well as to investigate the adsorptive/desorptive behavior of the collected organics.

The results shown here are consistent with results from preliminary experiments in both Berkeley and Anaheim using the filter pack technique, indicating that over a period of several days, the physical transfer of carbonaceous aerosol by liquid flow is not significant.

REFERENCES

1. W. Cautreels and K. Van Cauwenberghe, Atmos. Environ., 12, 1133 (1978).

2. P. W. Jones, R. D. Giammar, P. E. Strup and T. B. Stanford, Environ. Sci. Technol., 10, 806 (1976).

3. L. Van Vaeck and K. Van Cauwenberghe, Atmos. Environ., 12, 2229 (1978).

4. H. Della Fiorentina, F. De Wiest and J. De Graeve, Atmos. Environ., 9, 517 (1975).

5. P. K. Mueller, R. W. Mosley, and L. B. Pierce, "Carbonate and non-carbonate carbon in atmospheric particles," Proceedings of the 2nd International Clean Air Congress. New York, Academic Press (1970).

6. R. L. Dod, H. Rosen and T. Novakov, Lawrence Berkeley Laboratory Report, LBL-8696 (1979).

SURFACE CHARACTERIZATION OF FLYASH

S. Cohen, et al.

INTRODUCTION

Electron spectroscopy for chemical analysis (ESCA) can be used as a nondestructive surface-speciation technique. Not only can different elements be identified using ESCA, but information regarding chemical state--e.g., Fe(II) versus Fe(III)--is provided. Sample preparation is relatively simple, and only a small amount of sample--enough to dust over a piece of double-backed Scotch tape--is required. Provided that the signal can be distinguished from noise, ESCA therefore seems an ideal technique for characterizing a complex surface such as coal flyash. Two main difficulties of the technique are:

1. Matrix effects can be serious so that even comparison with model compounds will not give unambiguous assignment of ESCA peaks. In addition, a single element in flyash may exist in several chemical states and/or crystalline forms, thereby making peaks broad and diffuse and speciation difficult.

2. Of ultimate interest in flyash studies are the compounds released to the environment by leaching in waterways and the ease with which toxic substances in flyash are released in the respiratory tract at physiological pH. This is not strictly related to what species are initially on the flyash surface. The presence of pores, for instance, could enhance dissolution of species deep inside the flyash particle.

Solvent leaching studies should aid in these two problems and may even provide depth profiling information if the leachate is analyzed as a function of time. Unfortunately, complex equilibria in the extract probably mix the original salts and may cause precipitation where resulting mixtures are insoluble. For instance, $BaCl_2 + CaSO_4 \rightarrow BaSO_4\downarrow + CaCl_2$. Thus Ba^{2+} leached from the flyash in initially soluble form could precipitate and not be found in the leachate. Nevertheless, because solvent leaching when run in conjunction with ESCA studies may provide important surface information, and because solvent leaching may become an important technique in labs where ESCA is unavailable, the correlative study has been pursued.

D. F. S. Natusch has used "time resolved solvent leaching" to study flyash surfaces.[1] The method entails continuous leaching of the sample by a solvent, the leachate being analyzed as a function of time. The problems described above due to complex equilibria limited the study. The work described below is an attempt to develop the method proposed by Natusch.

EXPERIMENTAL

All ESCA work was done on an AEI spectrometer using the Al K_α (1486.6 eV) exciting line. Flyash samples were dusted onto a piece of double-backed Scotch tape. Scans were made over a 20-50 eV region (B.E. step = 0.2 to 0.5 eV for 100 channels) for times ranging from 10 seconds/channel for strong signals to 375 seconds/channel for very weak signals. Peaks were referenced to spectrometer hydrocarbon contamination with C(1s) = 284.6 eV.

Solvent extractions were done in acid-washed glassware by 15 minutes of ultrasonic treatment. In all cases, Barnstead deionized water was used to make up extracting solutions. Leachates were stored in acid-washed linear polyethylene containers, after filtering through an 0.2-μ pore-size Millipore filter.

Ion chromatography was done on a Dionex Model 14 ion chromatograph at a sensitivity of 10 μmho full scale. Atomic absorption work was performed on a Perkin-Elmer Model 360 atomic absorption instrument.

RESULTS AND DISCUSSION

Initial studies in this laboratory consisted of ESCA analysis of unleached flyash. Elements most strongly detected are listed in Table 1. Some information on chemical state was obtained, as can be seen by inspection of Figs. 1 and 2. Sulfur appears to be in the S(VI) form, in agreement with the work of Small.[2] Arsenic closely resembles the model compound As_2O_3; however, the similarity of As_2O_3 and As_2O_5 ESCA peaks will necessitate further work to confirm this hypothesis. Satellite structure, which yields information on both oxidation state and ligand environment, was faintly present for both Cu (Fig. 3) and Fe, but no assignments have yet been made.

The flyash was then leached by ultrasonic treatment. Compounds found in the leachate were compared with changes found on the flyash surface using ESCA. Because a flyash solution in water yields a basic pH (due to dissolution of CaO), both deionized water and dilute HNO_3 were used to vary extracting conditions. Leachate analyses are displayed in Table 2.

Although most of the initial leachate analyses were qualitative, some quantitative information was obtained. Ba^{2+} was detected at a concentration equal to the solubility limit of $BaSO_4$ in the H_2O leachate. This is precisely the result expected if the sparingly soluble salt $BaSO_4$ precipitates out of the wash. In every case examined, the nitric acid was found to be a better extractant than H_2O.

Inspection of flyash surfaces after sonication provided good correlation for some species; Figure 4 shows the effect of H_2O and acid washes on the flyash surface. Because ESCA is a relative, and not an absolute, technique, in order to compare peak intensities from separate samples it is advisable to normalize to a flyash constituent unaffected by the washes. Since even the matrix elements Fe, Si, and Al are found in the HNO_3 leachate, no reliable reference could be selected. Hence the intensities are listed in Fig. 4 as simply counts/sec/channel (unnormalized). The trends observed are nevertheless considered significant since: 1) the extent of the differences is too large to be caused by sample orientation in the spectrometer or thoroughness of coverage of the Scotch tape,

Table 1. Elements detected on untreated flyash surfaces by ESCA.

Transition metals	Cu, Cr, Fe
Alkaline and alkaline earth	Ba, Ca, Na
Other	Al, As, C, Cl, O, P, S, Si

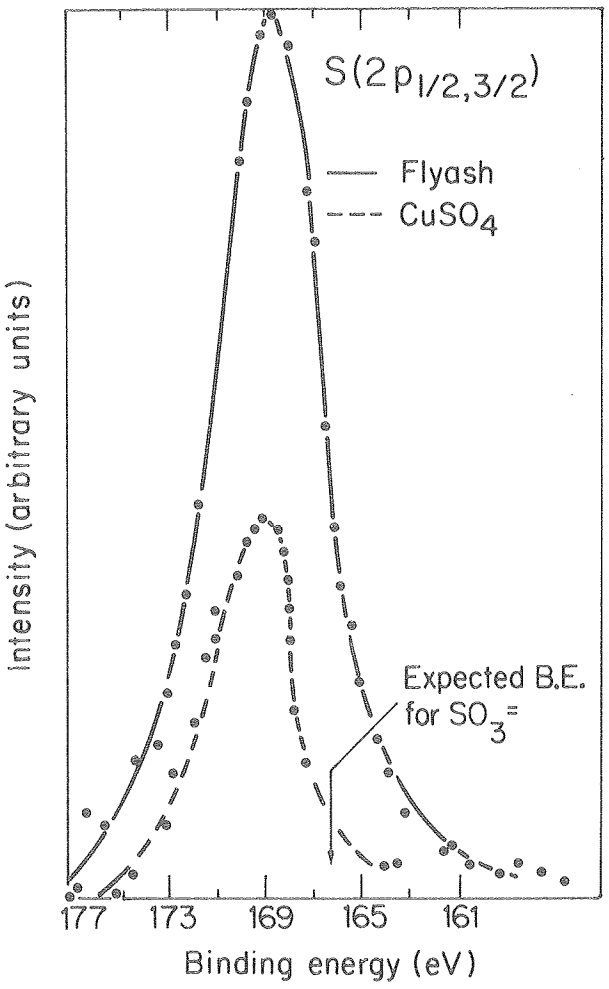

Fig. 1. Comparison of a flyash ESCA spectrum in the sulfur $2P_{1/2,\ 3/2}$ region to that of reagent-grade $CuSO_4$. If S^{+4} species were present, a shoulder should be observed in the position indicated. Binding energies in this and all ESCA spectra shown are referenced to spectrometer hydrocarbon contamination at 284.6 eV.

(XBL 801-43)

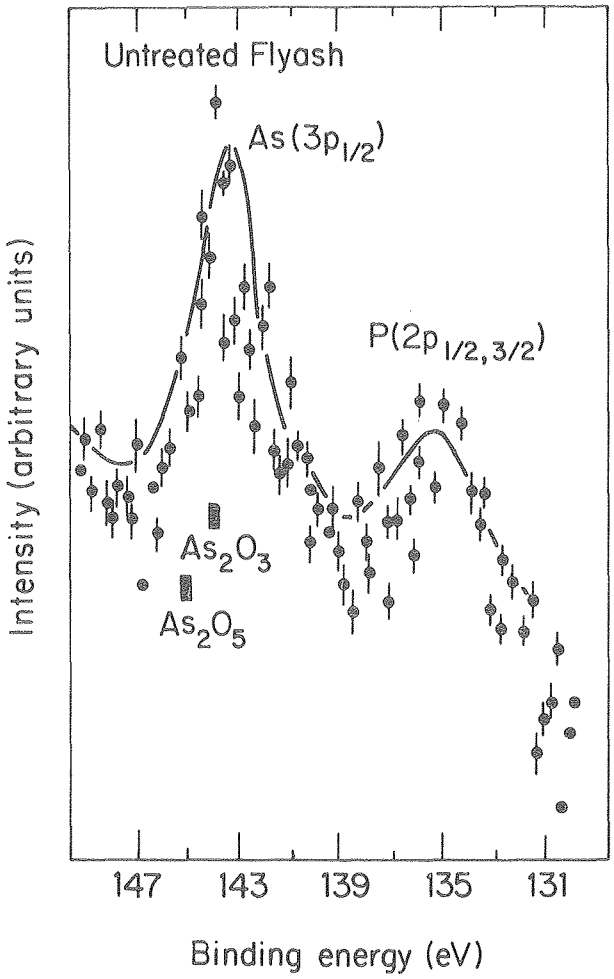

Fig. 2. ESCA spectrum of untreated flyash in the As $3P_{1/2}$ region. Positions of this peak for As_2O_3 and As_2O_5 are indicated. The peak at ~135 eV is due to phosphate ($2P_{1/2,3/2}$). It was removed by both water and acid wash.
(XBL 801-44)

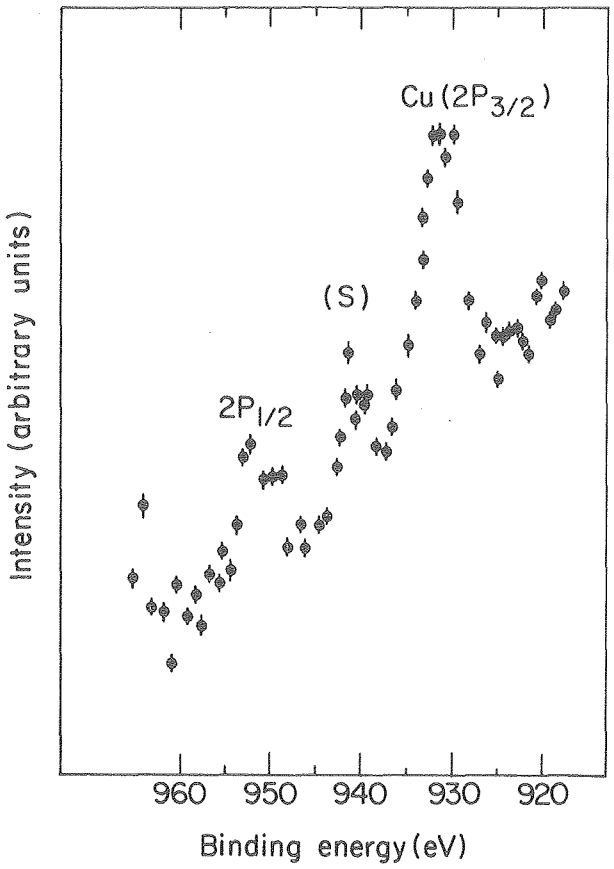

Fig. 3. Cu $2P_{1/2}$, $2P_{3/2}$ peaks and satellite structure (s) as indicated. (XBL 801-45)

Table 2. Species found in leachate from flyash.

	H_2O wash	Acid wash
Anions	SO_4^{2-}	SO_4^{2-}, F^-, Cl^-
Cations (Fe, Ba, Cu, Al, Si)[a]		
	Ca^{2+}, Na^+, K^+	Ba^{2+}, Ca^{2+}, Na^+, K^+, Mg^{2+}

[a]These elements were determined using AA; all other entries in the table provided by I.C.

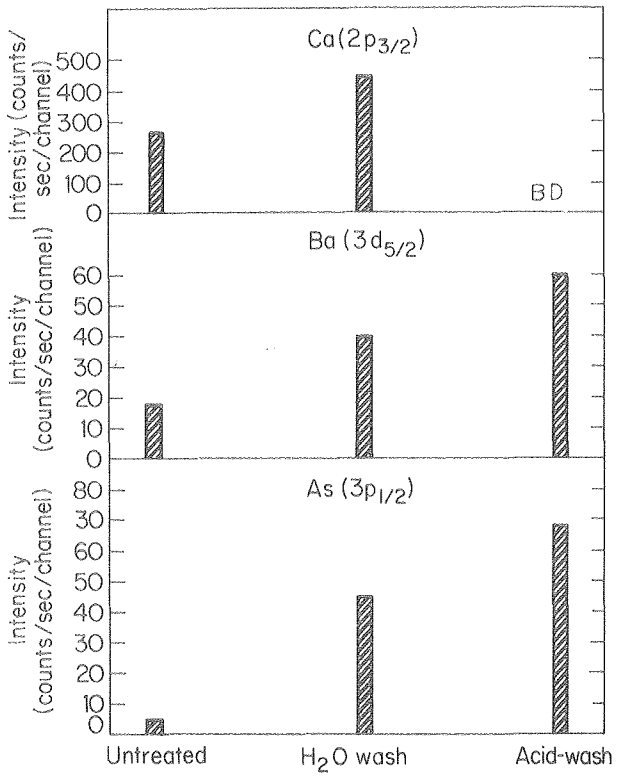

Fig. 4. Bar graphs showing the effect of water and acid wash on the (a) Ca (b) Ba and (c) As surface concentrations on flyash. The peak monitored is as indicated. The calcium peak was below detection for the acid-washed sample.
(XBL 801-46)

and 2) the trends shown in Fig. 4 were found to be reproducible.

As expected from the large amount of Ca^{2+} found in the nitric acid leachate, the acid wash completely removes Ca^{2+} from the surface. The surface enhancement of Ca^{2+} by the water-wash is rather unexpected, since the leachate results (Table 2) indicate the flyash has been depleted of Ca^{2+}. Keeping in mind that ESCA is a surface, not a bulk technique, we may be observing a novel surface adsorption of the Ca species onto the flyash surface as leaching from the interior proceeds. Enhancement of As and Ba on the flyash surface is effected by acid and water washes (Fig. 4). Presumably formation of insoluble compounds $BaSO_4$ and $FeAsO_4$, which precipitate onto the surface, explains this enhancement.

CONCLUSION

The investigation of flyash surfaces by combining ESCA and solvent leaching may prove to be a valuable analytical tool. The example of barium provides an indication of the strength of the method. Whereas detection of Ba^{2+} in the H_2O leachate at the concentration limit of $BaSO_4$ does not by itself provide conclusive evidence of $BaSO_4$ formation, enhancement of Ba in the ESCA spectrum supports such a conclusion. The latter observation also indicates that $BaSO_4$ is not initially present but is formed during the wash. In transition metals, changes in satellite structure could similarly be used to monitor transformation among various metal salts.

Future work will examine the hypothesis of time-resolved solvent leaching for both surface and matrix elements. Fe, Al, and Si are known to be distributed throughout the flyash matrix;[3] hence they would be expected to show constant concentration vs time profiles. In addition, surface concentrations of these species should not vary significantly with time. As, Cu, and Cr, however, which show surface enrichment, should yield observable changes in both the leachate profiles and surface studies.

REFERENCES

1. D. S. Natusch and M. Tomkins, private communication, July, 1979.

2. J. A. Small, An Elemental and Morphological Characterization of the Emissions from the Dickerson and Chalk Point Coal-fired Power Plants, Ph.D. thesis, University of Maryland (Chemistry) 1976.

3. R. L. Davidson, D. F. S. Natusch, J. R. Wallace, and C. A. Evans, "Trace elements in flyash dependence of concentration on particle size," Environ. Sci. Technol. 3, 1107 (1974).